Alma Mater Studiorum Università di Bologna
Archivio istituzionale della ricerca

Preference for locomotion-compatible curved paths and forward direction of self-motion in somatomotor and visual areas

(Article begins on next page)

27 September 2024

Preference for locomotion-compatible curved paths and forward direction of self-motion in somatomotor and visual areas

Sara Di Marco [a, b*], Patrizia Fattori [c], Gaspare Galati [b, d], Claudio Galletti [c], Markus Lappe [e, f], Teresa Maltempo [a, b], Chiara Serra [a, b], Valentina Sulpizio [b, c], Sabrina Pitzalis [a, b]

[a] Department of Movement, Human and Health Sciences, University of Rome ''Foro Italico'', Rome, Italy
[b] Department of Cognitive and Motor Rehabilitation and Neuroimaging, Santa Lucia Foundation (IRCCS Fondazione Santa Lucia), Rome, Italy
[c] Department of Biomedical and Neuromotor Sciences, University of Bologna, Bologna, Italy
[d] Brain Imaging Laboratory, Department of Psychology, Sapienza University, Rome, Italy
[e] Institute for Psychology, University of Muenster, Muenster, Germany
[f] Otto Creutzfeldt Center for Cognitive and Behavioral Neuroscience, University of Muenster, Muenster, Germany

---

*Correspondence:

Sara Di Marco, PhD

Department of Movement, Human and Health Sciences

University of Rome ''Foro Italico''

00194 Rome (Italy)

phone: 0039-06.36733.383

fax: 0039- 06.36733.387

e-mail: contact.saradimarco@gmail.com

Abstract

During locomotion, leg movements define the direction of walking (forward or backward) and the path one is taking (straight or curved). These aspects of locomotion produce characteristic visual motion patterns during movement. Here, we tested whether cortical regions responding to either egomotion-compatible visual motion, or leg movements, or both, are sensitive to these locomotion-relevant aspects of visual motion. We compared a curved path (typically the visual feedback of a changing direction of movement in the environment) to a linear path for simulated forward and backward motion in an event-related fMRI experiment. We used an individual surface-based approach and two functional localizers to define (1) six egomotion-related areas (V6+, V3A, intraparietal motion area [IPSmot], cingulate sulcus visual area [CSv], posterior cingulate area [pCi], posterior insular cortex [PIC]) using the flow field stimulus and (2) three leg-related cortical regions (human PEc [hPEc], human PE [hPE] and primary somatosensory cortex [S-I]) using a somatomotor task. Then, we extracted the response from all these regions with respect to the main event-related fMRI experiment, consisting of passive viewing of an optic flow stimulus, simulating a forward or backward direction of self-motion in either linear or curved path. Results showed that some regions have a significant preference for the curved path motion (hPEc, hPE, S-I, IPSmot) or a preference for the forward motion (V3A), while other regions have both a significant preference for the curved path motion and for the forward compared to backward motion (V6+, CSv, pCi). We did not find any significant effects of the present stimuli in PIC. Since controlling locomotion mainly means controlling changes of walking direction in the environment during forward self-motion, such a differential functional profile among these cortical regions suggests that they play a differentiated role in the visual guidance of locomotion.

Keywords: optic flow; steering; translation and rotation; PEc; fMRI

1. Introduction

While moving in the environment, the retina receives a visual feedback of self-motion, producing a source of visual information known as the optic flow (Gibson, 1950). This visual pattern is an essential cue for determining components of self-motion (egomotion; Gibson, 1950; Warren, 1998; Lappe et al., 1999; Britten, 2008) and for guiding locomotion through the external environment (Bremmer, 2011; Li and Warren, 2002; Li et al., 2011; Li and Cheng, 2011b).

When one travels on a straight path (pure body translation), heading (i.e., the instantaneous direction of self-motion) coincides with the path trajectory (Figure 1A). In such a case, heading estimation is sufficient to determine the direction of self-motion (Warren et al., 1988; Li and Cheng, 2011b). Under more complex but natural conditions, for example when one travels on a curved path (body translation and rotation), the optic flow becomes richer in information. The rotational component of self-motion produces additional visual motion that disturbs the simple radial pattern such that heading, instead of being identical to the straight path, is aligned to the tangent of the path trajectory (Regan & Beverly, 1982; Warren and Hannon, 1990; Lappe et al., 1999; Li and Cheng, 2011a) (Figure 1B). Thus, while in the case of the straight path heading keeps constant in retinotopic and allocentric coordinates, in the case of the curved path heading still remains constant in retinotopic coordinates but changes over time in allocentric coordinates. Yet, the retinal motions of the optic flow still specify the direction of self-motion, and computational models have shown how heading can be recovered from the retinal flow (Lappe and Rauschecker, 1993; Perrone and Stone, 1994; Beintema and van den Berg, 1996). However, when travelling on a curved path, the recovery of heading alone is not sufficient to estimate the future direction of self-motion. Instead, it is also necessary to estimate path curvature, which describes how the self-motion direction in the world changes over time. Psychophysical studies in humans have shown that both heading (Stone & Perrone, 1997; Li and Cheng, 2011a) and path curvature (Cutting et al., 1997; Warren et al., 1991; Bertin et al., 2000; Li et al., 2009) can be recovered from optic flow.
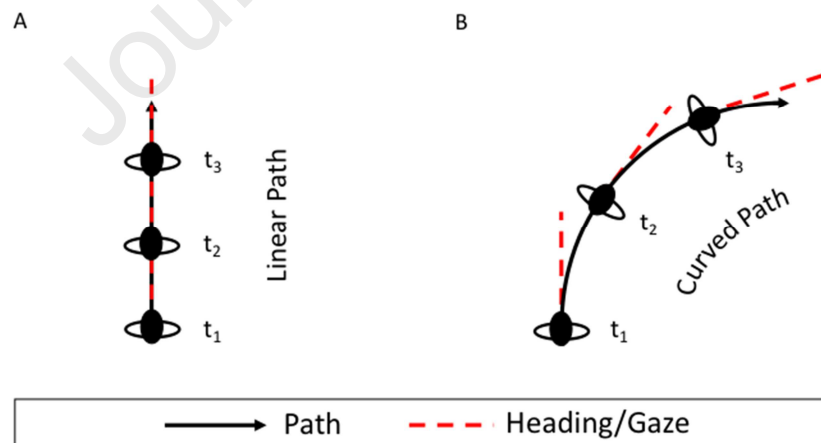
Figure 1. Schematic representation of the relationship between path (black arrow) and heading/gaze (red dashed line) for linear and curved path conditions. (A) Linear Path. Heading/gaze is aligned along the same direction as the path and keeps constant over time in both retinotopic coordinates and allocentric coordinates (with respect to the environment). (B) Curved Path. As in Linear Path condition, heading/gaze is the same in retinotopic coordinates. However, unlike in panel A, at any instance of time, heading/gaze is aligned to the tangent of the path and both heading and the future direction of self-motion (which is defined by the path curvature) change over time in allocentric coordinates.

Extensive physiological studies of visual sensitivity to optic flow have been made in non-human primates, mostly focusing on heading during linear motion. In monkeys, several areas are

3

selectively activated by egomotion-compatible optic flow, including MST, VIP, VPS, V6 and pmCSv (e.g., Cottereau et al., 2017). Most of them respond to flow components (Tanaka and Saito 1989; Duffy and Wurtz 1991; Paolini et al., 2000) and have been proposed to participate in heading encoding since their neurons are selective for the position of the focus of expansion (FOE) during forward and backward motion on a straight path (Duffy and Wurtz 1995; Lappe et al., 1996; Bremmer et al. 2002; Chen et al., 2011a,b; Fan et al., 2015). In addition to these areas, also the sensorimotor area PEc in the superior parietal lobule has been found to participate in heading encoding. This region, in addition to somatosensory neurons particularly sensitive to passive joint manipulation of both arm and leg (Breveglieri et al., 2006; 2008; Gamberini et al., 2018), contains direction-selective visual neurons with large receptive fields (Battaglia-Mayer et al., 2001; Squatrito et al., 2001; Breveglieri et al., 2008; Gamberini et al., 2018) sensitive to radial optic flow and to the position of the FOE (Battaglia-Mayer et al., 2001; Raffi et al., 2002; 2010; 2011; 2014). Specifically, most of the optic flow-responsive neurons respond to forward and backward motion on a straight path and show a preference for eccentric positions of the FOE (i.e., shifted with respect to the fixation). These pieces of evidence together suggest that PEc is involved in optic flow processing and heading encoding with the aim of coordinating lower limb movements during locomotion (Breveglieri et al., 2008; Bakola et al., 2010; Gamberini et al., 2018; Raffi et al., 2002; 2010; 2014). While many studies in monkeys have shown selectivity for heading during straight movement in many different areas, only one study has investigated changes in heading (and other flow components) such as occurring on a curved path (Paolini et al., 2000). That study found that responses in MST are determined by the instantaneous flow field (heading) and do not carry information about changes in the flow.

In humans, fMRI studies investigating the neural basis of heading encoding found that some egomotion-related visual regions (e.g., V6, VIP, CSv and PIC) but not others (V3A) showed greater activation for passive observation of visual motion stimuli simulating continuous changes in heading direction than for unchanging heading (Furlan et al., 2014; Huang et al., 2015). Other fMRI studies have investigated the neural correlates of future path encoding aimed at anticipating heading changes (Field et al., 2007; Billington et al., 2010, 2013). Surprisingly, so far little attention has been devoted to the relationship between heading and path curvature.

Previous human fMRI studies on heading encoding focused on cortical regions classically associated with visual egomotion processing, ignoring the possible contribution of sensorimotor regions that control lower limb movements. Notably to this regard, in recent fMRI studies we revealed that, while the egomotion cortical regions V6+, V3A and IPSmot do not respond to long-range leg movements, the egomotion areas CSv, pCi, PIC (Serra et al., 2019) and the newly defined human homologues of macaque PEc and PE (even if at different extent) (Pitzalis et al., 2019) respond to both optic flow and long-range leg movements. These findings suggest an involvement of these regions in optic flow processing with the aim of coordinating lower limb movements during locomotion. Although the visual properties of hPEc and hPE and their sensitivity to heading are still not investigated, the macaque and human evidence accumulated so far foster the hypothesis that hPEc (and maybe also hPE), together with CSv, pCi and PIC, play a critical role in the visual guidance of locomotion by integrating somatomotor and visual signals during movement in the environment. Table 1 lists all the acronyms used in the paper to indicate macaque and human brain regions.

Macaque	
MST	Medial Superior Temporal area
VIP	Ventral IntraParietal area

VPS	Visual Posterior Sylvian area
pmCSv	putative macaque Cingulate Sulcus visual area
PE and PEc	P stands for Parietal, E stands for the specific parietal area 'E' based on the von Economo and Koskinas classification (1925); c stands for caudal

Human	
CSv	Cingulate Sulcus visual area
PIC	Posterior Insular Cortex
IPSmot	IntraParietal motion area
pCi	posterior Cingulate area
hPE and hPEc	human PE and human PEc
S-I	Primary Somatosensory Cortex

Table 1. This table lists all the acronyms used in the paper to indicate macaque and human brain regions.

In order to assess whether and how sensitivity to egomotion-compatible optic flow of the above-mentioned regions is used in the visual guidance of locomotion, here we further explored their visual properties by verifying their response to locomotion-relevant visual motion parameters, such as path trajectory and direction of motion.

To this aim, we used a combined approach of individual surface-based analysis, task-evoked activity and an event-related paradigm by fMRI. Specifically, we independently defined on each individual surface two sets of regions using two dedicated functional localizers. As a first step, we defined the three leg-related cortical regions hPEc, hPE and the adjacent somatosensory primary cortex (S-I) by using the same somatomotor task we recently employed in Pitzalis et al. (2019), and identified a set of egomotion-related visual areas by using the flow field stimulus (Pitzalis et al., 2010) which has been recently proposed as the functional localizer for at least six regions including V6+, V3A, IPSmot, CSv, pCi and PIC (Serra et al., 2019). Afterwards, we examined the response of all these regions with respect to the main fMRI heading experiment, consisting of passive viewing of an optic flow stimulus, simulating forward and backward self-motion on either a linear or a curved path. We simulated locomotion-compatible visual feedback by presenting dot patterns moving along a ground plane, which is known to be particularly relevant in providing visual information relative to self-motion during locomotion (Marigold, 2008; Marigold and Patla, 2008). Finally, we employed a representational similarity analysis in both sets of regions to examine the neural representation underlying different directions and paths of visual motion. Based on macaque evidence of a large number of direction selective visual neurons in some of the above-mentioned motion areas (as V6+; Galletti et al., 1996; Gamberini et al. 2011), we expected to find different neural representations for forward and backward motion and that directions of motion closer in physical space entailed activity patterns more similar in neural representational space.

2. Materials and Methods

No part of the study procedures or analyses was preregistered prior to the research being conducted. We reported how we determined our sample size, all data exclusions (if any), all inclusion/exclusion criteria, whether inclusion/exclusion criteria were established prior to data analysis, all manipulations, and all measures in the study.

2.1   Participants

Twenty-eight healthy subjects participated in the study (mean age: 24, SD = 4.87, 17 males). All subjects had normal or corrected-to-normal vision and no previous history of psychiatric or neurologic disease. All participants were right-handed and right-footed, as assessed by the Edinburgh handedness inventory (Oldfield, 1971). These inclusion criteria were established prior to data collection and analyses. All subjects gave written informed consent. The protocol was approved by the Ethics Committee of Fondazione Santa Lucia, Rome, Italy. The sample size was determined based on previous similar fMRI studies (Field et al., 2007; 2015; Furlan et al., 2014). All subjects participated in two functional magnetic resonance imaging (fMRI) acquisition sessions in separate days, the first one to perform the main 'Heading' experiment and the second one to perform two localizer scans to map three leg-related somatomotor areas (hPEc, hPE and S-I) and six egomotion-related visual regions (V6+, CSv, pCi, IPSmot, PIC and V3A), respectively. For a subsample of subjects, localizer scans used to map the somatomotor regions were also included in the data set of Pitzalis et al. (2019).

2.2   Heading experiment

In the main event-related fMRI experiment, hereafter called *heading experiment*, the visual motion stimulus consisted of a virtual 3D environment with blue-sky filling the upper visual field and a black ground plane filling the lower visual field (Figure 2). A white central fixation cross, corresponding to the observer gaze direction during the simulated egomotion, was placed slightly above the horizon line. White dots moved along the black ground plane in an incoherent (random condition) or a coherent manner, so as to reproduce a locomotion-compatible optic flow and give participants the impression they were walking on the ground. Dots size and local speed appeared scaled along both distance and eccentricity dimensions as seen from the observer's point of view. Dots traveled with an average speed of 2°/s. Dots were randomly generated online at each scan and produced a continuous flow across trials, changing direction and path trajectory accordingly with experimental conditions. Four different coherent motion conditions were presented, as a result of a 2 x 2 factorial design (Figure 2A) with Direction (forward, backward) and Path (linear, curve) of the dots flow as factors:

1. the "Forward_Linear" condition simulated observer forward motion on a linear path with the gaze direction along the path;
2. the "Forward_Curve" condition simulated observer forward motion on a clockwise or counterclockwise curved path with the gaze direction tangential to the path;
3. the "Backward_Linear" condition simulated observer backward motion on a linear path with the gaze direction along the path;
4. the "Backward_Curve" condition simulated observer backward motion on a clockwise or counterclockwise curved path with the gaze direction tangential to the path.

An additional condition (the "Random" condition) was included as a high-level baseline. In this condition each dot moved in a different, randomly selected direction, so as to generate an incoherent visual motion pattern on the ground.

6
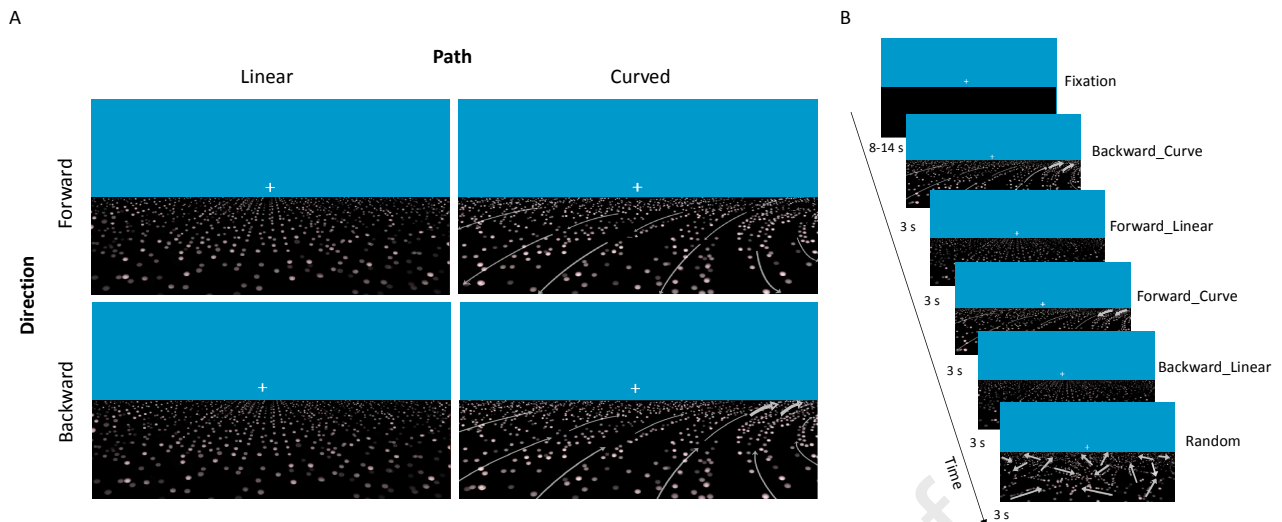
Figure 2. Visual stimuli and timeline used in the main experiment. (A) The panels show a schematic representation of the four coherent motion conditions organized according to a 2x2 factorial design, with Direction (forward, backward) and Path (linear, curve) as factors. Only for display purpose, grey arrows are superimposed on the stimulus in order to represent the direction of the visual motion on the black ground plane, as received on the retina during the self-motion. Note that the direction of visual motion is always opposite to the direction of the simulated observer. (B) Example of the 3s movie types for the four coherent (Forward_Curve, Forward_Linear, Backward_Curve, Backward_Linear) and Random motion conditions. Note that for display purpose only counterclockwise Forward_Curve and clockwise Backward_Curve are shown but also the opposite combinations were presented in the experiment.

In the four main experimental conditions, simulated gaze direction was along or tangential to the path, thus aligned with the instantaneous direction of self-motion (heading) (Figure 1). Throughout all conditions, participants held their gaze on the fixation point located just above the midpoint of the simulated horizon, so that the visual stimulation properly simulated their motion along the ground plane accordingly with experimental conditions. Indeed, linear visual feedback, as that used in the linear condition, is generated when heading/gaze is aligned with the linear path (Figure 1A), whereas curved visual feedback, as that used in the curve condition, is generated when heading/gaze keeps tangential to the curved path (Figure 1B). The condition of keeping gaze tangential to the curved path is known to provide good path estimates to human observers (Bertin et al., 2000; Saunders, 2010; Li & Cheng, 2011). Since gaze was aligned to heading in the four experimental conditions, heading was always in the screen center. For the linear motion condition this was also the direction of the path. In the curve conditions, in contrast, the path deviated to the left or right, depending on curvature direction. Hence, in the curve conditions there was no heading change in the retinotopic reference frame but changes in the direction of movement in the environment (allocentric reference frame) occurred over time.

In order to encourage good fixation and to maintain attention in a constant state diverted from the motion stimuli, a blink detection task was carried out at fixation. Participants were trained to detect a rare event, consisting of a blink of the fixation cross (lasting 50 ms and occurring a variable number of times, from 4 to 6, in each run). At the end of each scan, participants were asked to verbally report the number of times in which the fixation cross blinked. Behavioral responses were recorded, and subjects received feedback on their ability to maintain a steady fixation. We then calculated for each participant the percentage of correct responses averaged across scans. The percentage of correct responses averaged across subjects was equal to 97% (SD = 4.92), indicating a good capability of the participants to maintain fixation and a constant attentional state throughout all the *heading experiment.*

Each experimental condition lasted for 3 s (Figure 2B) and was randomly repeated twice within 30 s sequences of trials, which were separated by uniformly distributed 8, 10, 12 or 14 s long fixation periods (rest), in which no dots appeared along the black ground plane. Fixation periods constituted the low-level baseline in the study. Experimental conditions were repeated 16 times per scan. Each subject completed

four scans (except for two subjects who underwent three scans). This gave a total of 64 repetitions for condition.

2.3 Localizer scans

In a second set of fMRI experiments, localizer scans were conducted to define three leg-related regions (hPEc, hPE and S-I) based on the somatomotor task used in Pitzalis et al. (2019) and six egomotion regions (V6+, V3A, IPSmot, CSv, pCi and PIC) based on the visual motion task used in Serra et al. (2019). The specific procedures are described in detail below.

Somatomotor task (*Active Leg/Arm movement scans*). Subjects were instructed to execute long-range arm and leg movements, designed to maximally stimulate limbs joints and activate somatomotor neurons. Each scan consisted of seven arm and seven leg movement blocks lasting 20.5 s each, arranged in a pseudo-random sequence and interleaved with 14 fixation periods of variable duration (12, 14 or 16 s). Each block started with a written instruction ("FIX", "LEG" or "ARM") presented for 400 ms at the center of the screen to inform the participant on the task to be performed. During fixation blocks, subjects were asked only to maintain fixation throughout the block. Each arm and leg movement block included 4 consecutive trials as follows. Briefly, the white fixation cross turned red for 300 ms (warning signal for the movement preparation) and, after a variable delay (750, 1000, 1250, 1500 ms), turned green (go signal) for 4 s, instructing participants to execute a 4 s sequence of limb movement while keeping central fixation (see Pitzalis et al., 2019 for a detailed description). Before entering the scanner, participants were trained to correctly perform the task; then, in the scanner, they underwent a short warm-up phase to familiarize themselves with the set-up for leg movements in order to execute the movements as fluid as possible.

Visual motion task (*Flow Fields scans*). Participants passively observed eight 16-s blocks of coherently moving dot fields (dilations, contractions, spirals and rotations), interleaved with eight 16-s blocks of randomly moving dot fields, while maintaining central fixation. A new field of white dots was generated every 500 ms (dot size 0.4 x 0.4 deg^2). Dots immediately began to move along a trajectory so as to generate a coherent movement on a plane. The pattern motion was chosen randomly for that 500-ms period from a continuum ranging from dilation to outward spiral, to rotation, to inward spiral, to contraction. The center of the movement was jittered from flow to flow, and the dot speed was logarithmically scaled with eccentricity (average speed: 25°/s; range of speed variance: 17°/s- 33°/s). During the scrambled OFF period, dots and their movement vectors were generated as during the coherent ON periods except that each dot trajectory was rotated by a random angle around the pattern center before execution. This scrambled the coherency of movement (at a given point, dots moved in different directions) but preserved the speed gradient (central dots still moved slower than peripheral dots). The stimulus was presented in full view and has been described in detail also elsewhere (e.g., Pitzalis et al., 2010; Serra et al., 2019).

2.4 Experimental set-up

Subjects laid down on the scanner bed. In the somatomotor task, we used an in-house MRI-compatible set-up allowing subjects to perform controlled leg movements (see Pitzalis et al., 2019 for a detailed description). Briefly, it consisted of an aluminum track fixed via Velcro straps on a wooden table which perfectly fitted the scanner bed. The aluminum track ended with a foot aluminum support sliding along the whole track. In all tasks, the head alignment was held constant by a chin-neck rest to minimize movement during the scans. The chin-neck rest was constituted by a soft cervical collar, made of soft foam, supporting the subject' neck and chin. The cervical collar rested on the subject's chest greatly reducing head movements along the pitch axis (Pitzalis et al., 2019). The subject's head was stabilized with foam padding and additional foams were placed under the back and inion in order to reduce discomfort. In all tasks, visual stimuli were presented by a monitor placed at the end of the scanner bore and viewed by participants via a mirror mounted on the head coil. In the heading experiment, visual motion stimuli (subtending 23° (H) x 13° (V) in visual angle) were generated by using a combination of MATLAB (The MathWorks Inc., Natick, MA, USA), Psychtoolbox-3 (Brainard, 1997; Pelli, 1997) and OpenGL.

2.5 Image acquisition and preprocessing

MR images were acquired at the Santa Lucia Foundation (Rome, Italy) on a 3T Philips Achieva MR scanner using a standard head coil. Functional T2*-weighted images were collected using a gradient echo EPI sequence using blood-oxygenation level-dependent imaging (Kwong et al., 1992). Thirty-eight 3.6 mm slices were acquired in the AC–PC plane with an in-plane resolution of 2.5x2.5 mm and an ascending excitation order (0.4 mm gap), 72 x 69 image matrix, echo time (TE) = 30 ms, flip angle = 77°, repetition time (TR) = 2 s. From the superior convexity, sampling included all the cerebral cortex, excluding only the ventral portion of the cerebellum. In each scan, the first four volumes were discarded from data analysis to achieve a steady state, and the experimental tasks started at the beginning of the fifth volume. Overall, each subject completed two 526-s long somatomotor scans, two 256-s long visual motion scans (except one subject) and four 328-s long heading scans (only two subjects completed three scans). We also collected a T1-weighted 3D sequence for each participant using a turbo field echo sequence (TFE): TR = 13 ms, TE = 5.7 ms, flip angle = 8°, 256 x 228 image matrix, 0.5 x 0.5 mm in-plane resolution, 342 contiguous 0.5 mm thick sagittal slices.

Structural images were analyzed using FreeSurfer 5.1 (http://surfer.nmr.mgh.harvard.edu/) to obtain a surface representation of each individual cortical hemisphere in a standard space. We used the "recon-all" fully automated processing pipeline, which, among other steps, performs intensity correction, transformation to Talairach space, normalization, skull-stripping, subcortical and white-matter segmentation, surface tessellation, surface refinement, surface inflation, sulcus-based nonlinear morphing to a cross-subject spherical coordinate system, and cortical parcellation (Dale et al., 1999; Fischl et al., 1999a,b; Desikan et al., 2006). The resulting surface reconstructions were transformed to the symmetrical FS-LR space (Van Essen et al., 2012) using tools in the Connectome Workbench software (https://www.humanconnectome.org/software/get-connectome-workbench), resulting in surface meshes with approximately 74K nodes per hemisphere.

Functional images were realigned within and across scans to correct for head movement and coregistered with structural scans using SPM12 (Wellcome Department of Cognitive Neurology, London, UK). Functional data were then resampled to the individual cortical surface using ribbon-constrained resampling as implemented in Connectome Workbench (Glasser et al. 2013). Images for univariate analysis were then spatially smoothed using a 6-mm full-width at half-maximum (FWHM) isotropic Gaussian kernel. Representational similarity analysis (RSA) was performed on unsmoothed images. In order to reduce the impact of head movements on signal quality, the framewise displacement index (FD, Power et al., 2012) was quantified at each time point as an estimate in mm of head movement with respect to the previous time point and computed as the sum of the absolute values of the differentiated realignment estimates. FD values and six additional head movement-related regressors parameters (rotation and translation along the three axes x-y-z) were then used as nuisance regressors in BOLD analyses. The conditions of our ethics approval do not permit public archiving of the raw MRI data. The preprocessed MRI anonymous data are available upon request at the lead author Pitzalis S. Access will be granted after completion of a formal data sharing agreement and approval of the local ethics committee, in accordance with ethical procedures governing the reuse of sensitive data. The experimental stimuli are available at the following link: https://osf.io/kfsx2/?view_only=2cec50136d114173b59cf6213ad4172b.

2.6 Statistical Analyses of the fMRI data

Functional images were analyzed for each participant separately on a vertex by vertex basis, according to the general linear model as implemented in SPM12 (http://www.fil.ion.ucl.ac.uk/spm).

The analyses were conducted on two independently defined, theoretically motivated, sets of regions of interest (ROIs) (see below), i.e., leg-related and egomotion-related regions. All these regions were identified by analyzing data from the ''localizer'' scans in which active blocks were modeled as box-car functions, convolved with a canonical hemodynamic response function. On each individual hemisphere we defined three regions of interest (ROIs) on the left hemisphere from the somatomotor scans with a

9

significant response to leg movements relative to fixation (hPEc, hPE, S-I; see Figure 3A) and six bilateral ROIs from the visual motion scans with a significant response to coherently moving dots relative to random motion (V6+, V3A, IPSmot, CSv, pCi, PIC; see Figure 4A). Individual ROIs were created by selecting the most activated nodes, among supra-threshold cluster of activation (p < 0.05 FDR corrected at the cluster level, with a cluster-forming threshold of p < 0.001 uncorrected). We defined these regions by isolating separate activation peaks and their neighborhood through a watershed segmentation algorithm as applied to surface meshes (Mangan & Whitaker, 1999).

For the main experiment (*heading experiment*) analyses, we modeled each trial as a canonical hemodynamic response function time-locked to the trial onset. For each participant and region, we computed a regional estimate of the amplitude of the hemodynamic response, obtained by using a weighted spatial average across all vertices within each ROI of the surface-transformed unsmoothed BOLD time series. Separate regressors were included for each condition after subtracting the random motion condition (high-level baseline) from all the coherent motion conditions. The rationale behind this approach is to foster responses in regions which are highly sensitive to coherent motion compared to random motion. Parameter estimates representing signal change in each experimental condition were analyzed through a repeated-measures ANOVA, as detailed in the *Regions of interest (ROIs) definition and regional analysis* paragraph.

As a final step we performed a representational similarity analysis (Kriegeskorte, Mur, & Bandettini, 2008), in the above-mentioned regions, in order to evaluate the neural representation underlying the perception of different motion directions.

We used a general linear model (GLM) on unsmoothed time series, in which trials related to each exemplar of motion path (rightward curve, leftward curve, linear) within each direction (forward, backward) were modeled by separate regressors in order to estimate the magnitude of the response at each node for each exemplar and direction separately. For each region, we built a representational dissimilarity matrix (RDM) by computing multivariate distances, as an index of dissimilarity of neural representations, between the activity patterns associated with each pair of stimuli. The dissimilarity between them is measured as 1 minus the correlation (0 for perfect correlation, 1 for no correlation, 2 for perfect anticorrelation). We then averaged the RDM elements, within subjects, depending on whether they were computed on pairs of stimuli belonging to the same or to different direction (forward, backward). Since we observed that exemplars belonging to the same direction were more similar among them as compared to exemplars belonging to different directions, thus indicating the existence of different neural representations for forward and backward directions, we built separate RDM matrices for forward and backward conditions. Specifically, we computed for both forward and backward motion, a dissimilarity index, indicating the neural distance between leftward and rightward path curvature with respect to the linear path, as follows:

$$Df/b = LR - \frac{Lli + Rli}{2}$$

Where D f/b is the dissimilarity between leftward (L) versus rightward (R) path curvature and L (or R) versus the linear path (li), separately for forward (f) or backward (b) directions, respectively.

In both somatomotor and egomotion regions we tested whether D f/b was higher than zero using one-sample t tests. We also directly compared the two indexes (Df and Db), by using a 2-tailed t test. Bonferroni's correction for multiple comparisons was applied (p = 0.006, corresponding to p = 0.05/N, N = 9, number of regions).

2.7 Regions of interest (ROIs) definition and regional analysis

Individually defined ROIs

Leg-related regions from the somatomotor task. To localize regions responding to leg movements we looked at all the activation peaks in the dorsomedial somatosensory/parietal cortex as resulting from the Leg > Fixation contrast map. As recently described in Pitzalis et al. (2019), this procedure allows to define on the left hemisphere of most of the subjects three leg-related regions. As detailed in Pitzalis et al. (2019) the three regions were anatomically located as follow (Figure 3A): (1) hPEc (identified in 26/28 hemispheres, in the anterior part of the dorsal precuneus), (2) hPE (identified in 28/28 hemispheres, on the exposed dorsomedial surface of the anterior SPL, right over the dorsal tip of the cingulate sulcus) and (3) S-I (identified in 28/28 hemispheres, on the medial portion of the brain surface, anterior to the dorsal tip of the cingulate sulcus and posterior to the dorsal tip of the central sulcus). We defined ROIs only in the left hemisphere to account for the fact that participants used their right limbs.

Egomotion-related regions from the visual motion task. To localize areas selectively responsive to coherent optic flow, we compared the BOLD response to coherently versus randomly moving dots. As recently described in Serra et al. (2019) this stimulus allows to define six distinct cortical regions strongly and bilaterally responsive to egomotion-compatible stimuli. As detailed in Serra et al. (2019) the six regions were anatomically located as follow (Figure 4A): (1) V6+, identified in 52/54 hemispheres, in the dorsal most part of parieto-occipital sulcus, POs. Given that the here defined region may also include the more anterior V6Av, which was found to respond to this visual motion task as well (Pitzalis et al., 2013a; Tosoni et al., 2015), here we refer to this region as V6 complex (or V6+); (2) V3A, identified in 49/54 hemispheres, in the ventral portion of the posterior intraparietal sulcus, IPs; (3) IPSmot, identified in 37/54 hemispheres, along the dorsal segment of the IPs; (4) pCi, identified in 35/54 hemispheres, within the posterior dorsal tip of the cingulate sulcus; (5) CSv, identified in 48/54 hemispheres, in the depth of the posterior part of the cingulate sulcus, anterior to the posterior ascending portion of the cingulate sulcus; and (6) PIC, identified in 44/54 hemispheres, at the junction between the posterior insula and the posterior parietal cortex. We defined each ROI bilaterally and then the mean percent signal change estimated in each ROI and each participant for each experimental condition was averaged across both hemispheres.

In order to test these ROIs with respect to the main experiment of the present study (*heading experiment*), regional hemodynamic responses were analyzed through a 2 x 2 repeated-measures ANOVA that allowed us to explore ROIs sensitivity to two locomotion-relevant visual parameters in the optic flow, namely Direction (forward, backward) and Path (linear, curve). In this ANOVA, we used a Bonferroni correction for multiple comparisons.

3. Results

In order to verify whether cortical regions responding to either egomotion-compatible visual motion or leg movements (or both) are also sensitive to path curvature and/or to the direction of self-motion (forward, backward), we studied two sets of theoretically motivated regions of interest defined by using dedicated functional localizers (see Methods, paragraph 2.3 for details).

As a first step, we used the somatomotor task to define three leg-related somatomotor areas (hPEc, hPE, S-I) as recently described in Pitzalis et al. (2019). Figure 3A shows the average location of these three regions, projected onto an inflated representation of a standard brain.

As a second step, we used the visual motion task to define six egomotion-related visual areas (V6+, pCi, CSv, V3A, IPSmot, PIC) as recently described in Serra et al. (2019). Figure 4A shows the average location of these six regions, projected onto an inflated medial and lateral representation of a standard brain.

Table 2 reports MNI coordinates of the peaks of all individually defined regions, averaged across subjects, the extent (number of nodes) and the mean peak t-value for each region.

Region		MNI coordinates				
	Hemisphere	X	Y	Z	Number of nodes	Peak T-value
hPEc	LH	-16 ± 5	-50 ± 3	66 ± 3	268 ± 172	10.69 ± 4
hPE	LH	-11 ± 2	-42 ± 2	68 ± 5	316 ± 172	17.11 ± 7

S-I	LH	-5 ± 2	-36 ± 5	62 ± 5	238 ± 91	17.57 ± 6
V6+	LH	-16 ± 3	-81 ± 5	36 ± 6	156 ± 101	8.93 ± 3
	RH	20 ± 2	-78 ± 4	37 ± 7	202 ± 102	9.58 ± 3
V3A	LH	-24 ± 5	-81 ± 8	25 ± 7	275 ± 211	7.85 ± 3
	RH	27 ± 4	-80 ± 7	25 ± 8	253 ± 181	7.44 ± 2
IPSmot	LH	-26 ± 4	-59 ± 4	56 ± 4	142 ± 82	7.37 ± 2
	RH	27 ± 4	-55 ± 6	56 ± 6	128 ± 87	6.12 ± 1
pCi	LH	-13 ± 3	-44 ± 4	52 ± 4	130 ± 102	6.34 ± 2
	RH	12 ± 3	-42 ± 5	51 ± 5	156 ± 162	6.42 ± 3
PIC	LH	-44 ± 5	-37 ± 4	18 ± 5	117 ± 105	5.39 ± 1
	RH	50 ± 10	-32 ± 2	20 ± 5	131 ± 104	6.08 ± 2
CSv	LH	-11 ± 3	-23 ± 5	40 ± 3	118 ± 79	6.13 ± 1
	RH	13 ± 2	-23 ± 6	42 ± 3	140 ± 96	6.04 ± 2

Table 2. MNI coordinates (mm) of ROIs defined using dedicated localizers. The peaks of individually defined regions are reported, as values mediated across subjects. Size: mean number of nodes (± standard deviation). Statistical significance: mean peak t-value (± standard deviation).

We then studied the functional response profile of the resulting nine areas (hPEc, hPE and S-I, V6+, V3A, IPSmot, CSv, pCi and PIC) during the Heading experiment to explore their sensitivity to path curvature as well as to the self-motion direction. The mean percent signal change observed in each of these regions for the four visual motion conditions presented in the heading experiment is plotted in the column histograms of Figures 3B,C,D and 4B. To reveal any significant path- or direction-related differences between conditions, beta values underwent an ANOVA with Direction (forward, backward) and Path (linear, curve) as factors, according to a 2x2 factorial design (where the random condition was subtracted out from each of the four coherent motion conditions).

Results are separately described below for each set of ROIs. In Figures 3A and 4A each ROI is color-coded based on ANOVA results and only the left hemisphere of each brain is shown to account for the presence of left hemisphere-only defined regions (hPEc, hPE, S-I).

As to the three somatomotor regions, plots in Figure 3B,C,D show a significant main effect of Path in all regions (blue-colored) with higher responses for Curved Path compared to Linear Path (hPEc: $F_{1, 25}$ = 6.90, p = 0.014, η_p^2 = 0.216; hPE: $F_{1, 27}$ = 7.36, p = 0.011, η_p^2 = 0.214; S-I: $F_{1, 27}$ = 5.78, p = 0.023, η_p^2 = 0.176) but not a significant main effect of Direction (hPEc: $F1,25$ = 2.63, p = 0.118; hPE: $F1,27$ = 0.49, p = 0.488; S-I: $F_{1, 27}$ = 0.11, p = 0.742). The interaction Direction by Path was not significant.
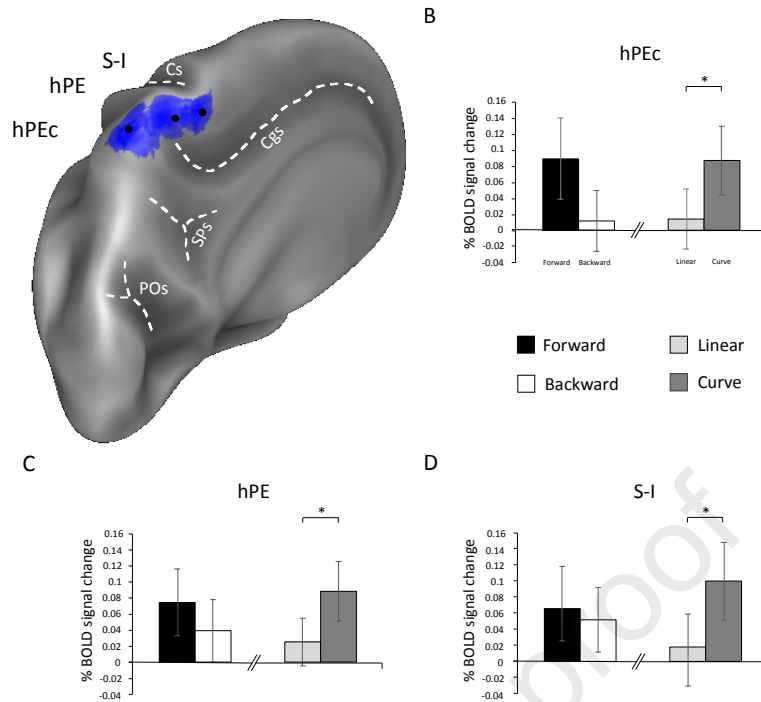
Figure 3. Response of leg-related somatomotor ROIs. (A) Overlap of the three individually defined leg-related ROIs rendered on the inflated representation of the left hemisphere of the Conte69 surface-based atlas. ROIs are blue-colored based on the ANOVA results, indicating that all regions (hPEc, hPE and S-I) showed the main effect of Path. The peaks of the ROIs are marked by a black spot. (B) Column histograms plot the mean percent signal change ± SE estimated in each leg-related somatomotor ROI and averaged across participants for the four visual motion conditions. Asterisks mark significant main effects. * $p < 0.05$; ** $p < 0.01$; *** $p < 0.001$. ROIs, regions of interest; POs, parieto-occipital sulcus, SPs, sub-parietal sulcus, Cgs, cingulate sulcus, Cs, central sulcus.
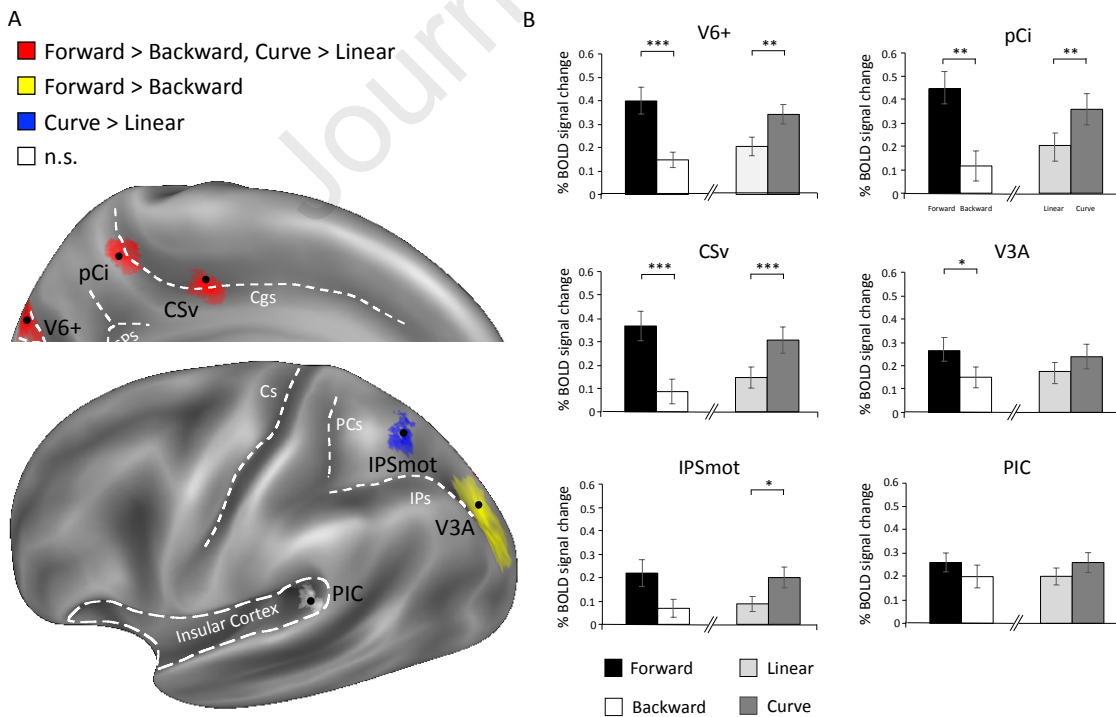
Figure 4. Response of egomotion-related visual ROIs. (A) Overlap of the six individually defined egomotion-related visual ROIs displayed on the inflated representation of the left hemisphere of the Conte69 surface-based atlas. ROIs colors indicate, as per ANOVA results, in red the egomotion visual areas showing both main effect of Direction and main effect of Path (V6+, CSv and pCi), in blue the egomotion visual area showing only the main effect of Path

13

(IPSmot), in yellow the egomotion visual area showing only the main effect of Direction (V3A) and in white the egomotion visual area not showing any effect (PIC). The peaks of the ROIs are marked by a black spot. Only the left hemisphere of the standard brain is shown but egomotion-related visual areas have been defined bilaterally. (B) Column histograms plot the mean percent signal change ± SE estimated in each egomotion-related visual ROI and averaged across participants for the four visual motion conditions. Asterisks mark significant main effects. * $p < 0.05$; ** $p < 0.01$; *** $p < 0.001$. ROIs, regions of interest; CSv, cingulate visual area; IPSmot, intraparietal motion area; pCi, posterior cingulate sulcus area; PIC, posterior insular cortex; V6+, V6 complex; POs, parieto-occipital sulcus, SPs, sub-parietal sulcus, Cgs, cingulate sulcus, Cs, central sulcus, PCs, post-central sulcus, IPs, intraparietal sulcus.

As to the six egomotion regions, plots in Figure 4B show differentiated functional profiles among them. In V6+, pCi and CSv (red-colored), we found both a significant main effect of Direction, with higher responses for Forward compared to Backward (CSv, $F_{1,24} = 18.89$, $p = 2.19 \times 10^{-4}$, $\eta_p^2 = 0.440$; pCi, $F_{1,20} = 16.42$, $p = 0.001$, $\eta_p^2 = 0.451$; V6+, $F_{1,26} = 17.55$, $p = 2.85 \times 10^{-4}$, $\eta_p^2 = 0.403$) and a significant main effect of Path, with higher responses for Curved Path compared to Linear Path (CSv, $F_{1,24} = 24.24$, $p = 5.1 \times 10^{-5}$, $\eta_p^2 = 0.502$; pCi, $F_{1,20} = 13.49$, $p = 0.002$, $\eta_p^2 = 0.403$; V6+, $F_{1,26} = 12.51$, $p = 0.002$, $\eta_p^2 = 0.325$). In V3A (yellow-colored), we found a significant main effect of Direction with higher responses for Forward compared to Backward ($F_{1,24} = 4.42$, $p = 0.046$, $\eta_p^2 = 0.156$) but not a significant main effect of Path ($F_{1,24} = 3.63$, $p = 0.069$), while in IPSmot (blue-colored), we found a significant main effect of Path, with higher response for Curved Path compared to Linear Path ($F_{1,21} = 6.30$, $p = 0.020$, $\eta_p^2 = 0.231$) but not a significant main effect of Direction ($F_{1,21} = 4.07$, $p = 0.057$, $\eta_p^2 = 0.162$). Finally, in PIC (white-colored), we found no significant effects for either Path ($F_{1,24} = 2.27$, $p = 0.145$) or Direction ($F_{1,24} = 1.12$, $p = 0.300$). The interaction Direction by Path was not significant.

To sum up, egomotion visual regions CSv, pCi and V6+ showed both main effects (Direction: Forward > Backward and Path: Curve > Linear; red-colored); somatomotor regions hPEc, hPE and S-I and egomotion region IPSmot showed the main effect of Path (Curve > Linear; blue-colored); and egomotion visual region V3A showed the main effect of Direction (Forward > Backward; yellow-colored). Egomotion visual region PIC did not show any significant effect (white-colored).

Finally, in order to characterize whether the neural patterns underlying the investigated directions of egomotion were different, i.e., how much a given exemplar "resembles" another one in terms of the underlying neural representation, we computed for each region the representation dissimilarity matrix (RDM) between pairs of stimuli (Figure 5), that is, the multivariate distances between the neural activation patterns evoked by each pair of stimuli, taken as indices of the diversity between them. We first grouped the elements of the matrix according to whether the two stimuli in the pair belonged to the same direction (forward, backward) or not. In all the investigated regions, we observed that exemplars belonging to the same direction (forward or backward) were more similar each other than exemplars belonging to different directions ($t_{15 < df < 27} \geq 9.84$; $p_s < 0.3^{-9}$).

We then explored whether directions of egomotion closer in physical space entailed activity patterns more similar in neural representational space. To this aim, we checked whether neural representations associated to exemplars belonging to closer directions (leftward or rightward vs the linear path) were more similar than those associated to exemplars belonging to more distant directions (leftward vs rightward).

We found that the dissimilarity index for forward direction was higher than zero in hPE ($t_{1,27} = 3.57$; $p = 0.001$), although a strong significant, but Bonferroni-uncorrected, effect was also observed in hPEc and S-I (hPEc: $t_{1,25} = 2.91$; $p = 0.007$; S-I: $t_{1,27} = 2.83$; $p = 0.008$). These results indicated that, among all the somatomotor regions, hPE, and, to lower extent, hPEc and S-I, are sensitive to the real distances between motion directions, i.e., the neural distance between leftward and rightward directions of motion along the curved path was higher than the distance between leftward (or rightward) motion direction and the linear path. We also found that this index was higher than zero in all the egomotion regions (CSv: $t_{1,22} = 3.64$; $p = 0.001$; PIC: $t_{1,21} = 5.37$; $p = 0.00001$; V6+: $t_{1,24} = 3.87$; $p = 0.0007$; V3A: $t_{1,24} = 3.42$; $p = 0.002$; IPSmot: $t_{1,18} = 3.17$; $p = 0.005$), although pCi showed a significant but Bonferroni-uncorrected result ($t_{1,16} = 2.48$ $p = 0.024$).

The dissimilarity index for backward direction was higher than zero only in S-I ($t_{1,27} = 3.42$; $p = 0.002$), while hPEc and hPE showed significant, but Bonferroni-uncorrected results (hPEc: $t_{1,25} = 2.72$; $p = 0.011$; hPE: $t_{1,27} = 2.34$; $p = 0.027$). With respect to the egomotion regions, we found that this index was significant in the

14

three most posterior regions V6+, V3A and IPSmot (V6+: $t_{1,24}$ = 5.15; p = 0.00003; V3A: $t_{1,24}$ = 5.16; p = 0.00003; IPSmot: $t_{1,18}$ = 3.26; p = 0.004), with marginal effects found in the pCi ($t_{1,16}$ = 2.48 p = 0.024) and CSv ($t_{1,22}$ = 2.35; p = 0.027), but not in PIC ($t_{1,21}$ = 1.90 p = 0.071), indicating that a distance-related representation was also present for backward direction, mainly in the "pure visual" egomotion regions, known to be not implicated in the visual control of locomotion (Serra et al., 2019).

The direct comparisons between the dissimilarity index for forward direction and the dissimilarity index for backward direction revealed no significant differences neither in somatomotor nor in egomotion regions ($t_{15 < df < 27}$ ≥ 2.12; p_s < 0.98), indicating that the neural distances between left and right motion direction along the curved path relative to the linear path are comparable for forward and backward directions.
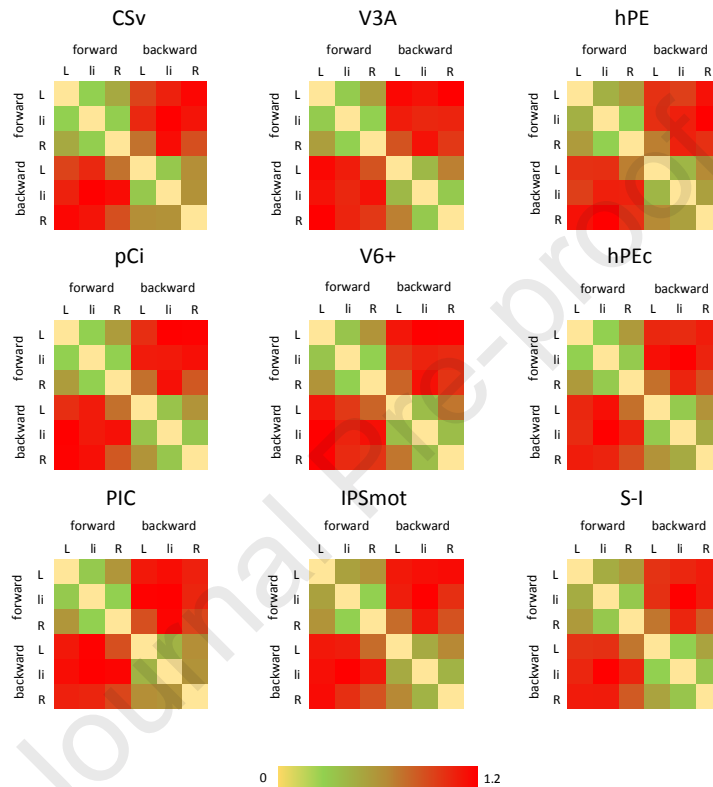
Figure 5. Representational dissimilarity matrices. Neural distances (1 minus correlation) between pairs of exemplars are plotted in green-to-red patches, for each ROI. RDM is symmetric about a diagonal of zeros. L, leftward curved path; li, linear path; R, rightward curved path.

4. Discussion

In the present study, two functional localizers and an event-related fMRI experiment were used to reveal whether leg-related somatomotor regions (hPEc, hPE, S-I) and egomotion-related visual areas (V6+, V3A, IPSmot, CSv, pCi, PIC) are differentially sensitive to locomotion-relevant aspects in the optic flow, namely path curvature (linear or curved) and self-motion direction (forward or backward). We found a differentiated functional profile among these areas, with some regions only preferring curved paths compared to linear paths (hPEc, hPE, S-I and IPSmot), one region only preferring forward direction of motion compared to backward direction (V3A), one region not showing any preference (PIC) and the others preferring both curved paths and forward direction (V6+, CSv and pCi).

Hereafter, we will first provide a description of the functional meaning of having or not a preference for each of the tested conditions. Then, regions will be grouped by their different

15

functional profiles and discussed taking into account previous evidence from macaque and human brain studies. Finally, we will suggest the possible functional roles played by these regions in the visual guidance of locomotion. We begin by preferences for path curvature.

A region preferring curved over linear paths is likely able to preferentially process visual information in the optic flow signaling changes in the direction of movement in the external visual world during self-motion. Indeed, when one wants to change direction during natural locomotion it is usually by walking on a curved path rather than by stopping, changing direction, and then starting walking. Thus, a region preferring curved over linear paths is likely involved in such a steering strategy. Moreover, areas responding preferentially to curved paths might also provide information about the future direction of self-motion by estimating path curvature, independently of direction. Indeed, when walking on a curved path, instantaneous heading is insufficient to estimate the future direction of self-motion and a measurement of path curvature from optic flow is required to determine how the self-motion in the world changes over time (Stone & Perrone, 1997; Li and Cheng, 2011a; Cutting et al., 1997; Warren et al., 1991; Bertin et al., 2000; Li et al., 2009, Saunders, 2010). This is an important information for steering, but also for locomotor stability. The centrifugal force during curved movement is directly related to the curvature, but not to the direction of travel along the curved path. Therefore, during locomotion on a curved path the center of mass of the body has to be adjusted depending on path curvature similarly for forward and backward movement. In contrast, a region not preferring curved over straight paths does not play a preferential role in processing changes of direction in the environment and future direction of self-motion. Such an area may signal for example the instantaneous heading as a current state of self-motion.

Also preferences for forward or backward motion suggest specific involvement in locomotion control, since these opposite directions convey very different information. Forward motion provides useful information about both the self-motion direction and the external visual world towards which we are moving (for example, differences in the speed of the optic flow convey information about the structure of the ground - bumps, holes, gutters -, stable obstacles or approaching objects). In contrast, backward motion is not informative about the visual environment behind us but only informs us about our direction (i.e. if we are moving backward, on a curved or a linear path) and visual stimuli from which we want to back off. In other words, during backward motion we have no visual feedback to prevent collisions with obstacles behind us or to anticipate postural adjustments necessary, for example, to not lose balance and fall down. Thus, a region not preferring either forward or backward motion may only be able to estimate the direction of self-motion. A region preferring forward over backward motion, instead, may be able to estimate self-motion direction as well, but it is also able to perform a 'fine' visual analysis of the environment in terms of global and local changes of luminance, contrast, texture and other parameters which are informative of the presence of ground irregularities (bumps, holes), static obstacles and dynamic objects (either approaching or not the observer). This deep visual analysis is necessary for the visual guidance of locomotion.

All somatomotor regions hPEc, hPE and S-I and egomotion visual area IPSmot (blue-colored regions in Figure 3A and 4A) show a preference only for curved over linear paths. The lack of a preference for forward motion in these regions indicates that hPEc, hPE, S-I and IPSmot are not implicated in a fine analysis of the visual features of the environment during self-motion. The lack of preference for forward direction in hPEc is in line with macaque data showing optic flow-sensitive neurons responding to both forward and backward visual motion (Battaglia-Mayer et al., 2001; Raffi et al., 2002; 2010; 2011; 2014). Taken together, these results suggest that hPEc, hPE, S-I and IPSmot are involved in encoding changes in the direction of self-motion in a wide range of

16

actions not only including locomotion (for example when moving backward and rotating our body in order to avoid an approaching object). This is in line with the specific functional properties of these regions. Indeed, hPEc, hPE and S-I are primarily somatomotor areas which contain, even if at a different extent, a somatosensory representation of the entire body (Pitzalis et al., 2019; Sulpizio et al., 2020a; Huang et al., 2012; Penfield, 1950). Hence, they are likely able to encode visual motion feedback of whole-body movements produced by joint stimulation in any direction, thus allowing them to control several kinds of limb movements in space during self-motion. Egomotion visual area IPSmot, likely corresponding to the human VIP as functionally defined by previous fMRI studies (Wall & Smith, 2008; Cardin & Smith, 2010; Furlan et al., 2014; Uesaki & Ashida, 2015; Serra et al., 2019), is a retinotopically organized polysensory region showing visual, somatosensory, auditory and vestibular responses (Bremmer et al., 2001; Sereno & Huang, 2006; Smith et al., 2012; Greenlee et al., 2016; Smith et al., 2017). Interestingly, this region is thought to be specialized for detecting looming objects around the face and guiding aggressive and defensive movements (Graziano & Cooke, 2006; Kaas et al., 2011; Huang et al., 2017). Specifically, the preference for curved motion in IPSmot is consistent with defensive movements implying rotation of the body in order to avoid approaching objects. Also the lack of a preference for forward or backward direction of motion, which are respectively associated with aggressive (or simply approaching) and defensive actions, is in line with the functional role proposed for this region (Huang et al., 2017). Finally, the encoding of curvature independent of direction could also be related to a role of these areas in locomotor stability as the physical forces during curved movement depend on the curvature but not on the direction.

Egomotion visual area V3A (yellow-colored region in Figure 4A) exhibits only a preference for forward motion, suggesting a fine visual analysis of the external world during locomotion. These results are both in line with the fact that V3A is an early extrastriate motion-sensitive visual region with a clear retinotopic organization (Tootell et al., 1997; Sunaert et al., 1999; Orban et al., 2003) which is able to perform a detailed analysis of the visual field and likely does not discriminate between two types of path curvature with different functional role, like curved and linear paths. Also, the lack of a preference for curved paths over linear paths is in line with results from Huang et al. (2015) showing that area V3A does not prefer heading changes.

Egomotion visual areas V6+, CSv and pCi (red-colored regions in Figure 4A) show a preference for both curved paths and forward motion, indicating that these regions are all implicated in heading changes and self-motion direction estimation, especially during locomotion. Such a fine visual analysis may also support locomotor stability during locomotion by allowing to anticipate postural adjustments. This is in good agreement with the fact that V6+ is an early extrastriate motion-sensitive visual area (Pitzalis et al., 2010; 2013a) which is retinotopically organized (Pitzalis et al., 2006) and is able to discriminate among different types of self-motion (i.e., translational, circular, radial and spiral motion, Pitzalis et al., 2013b). Also egomotion visual areas CSv and pCi (Antal et al., 2008; Wall & Smith, 2008; Cardin & Smith, 2010; Fischer et al., 2012; Furlan et al., 2014; Uesaki & Ashida, 2015; Field et al., 2015; Wada et al., 2016; Serra et al., 2019; Pitzalis et al., 2020) are good candidates for the analysis of self-motion aspects with different functional meanings. For example, CSv is a multisensory region receiving also vestibular input (Smith et al., 2012; Greenlee et al., 2016; Smith et al., 2017, 2018), indicating that this area participates in processing multimodal signals associated with whole-body motion. Moreover, CSv and pCi are located in the cingulate cortex which is known to participate in monitoring head and body movements in space during self-motion (Gitelman et al., 1999; Kim et al., 1999; Mesulam, 1999). Finally, retinotopic maps have been observed also in the portion of cortex hosting both CSv and pCi (Huang & Sereno, 2018), likely explaining their involvement in a fine analysis of the visual world. Notably, the CSv location seems to correspond to that of a recently reported retinotopic visual map in the anterior

17

cingulate region, referred to as anterior cingulate visual area (ACv; Sood et al., 2016), which according to the authors would correspond to the human equivalent of the dorsomedial FEF. In macaque, the dorsomedial frontal eye fields are attached to supplementary motor cortex and have more involvement in goal-directed saccades (e.g., relevant to locomotion) rather than the specific vector saccades seen in the (standard) lateral frontal eye fields.

Surprisingly, in human studies less attention has been devoted to sensitivity to locomotion-compatible curved path as compared to linear path and forward visual motion as compared to backward motion. The few previous fMRI studies (Furlan et al., 2014; Huang et al., 2015), partially consistent with present results, have shown that areas V6, V6Av, CSv, VIP, V3A, PIC and a cortical territory extending into the superior parietal lobule (SPL) and the anterior precuneus (aPCu), which may encompass hPEc, hPE and pCi, respond to visual motion stimuli simulating continuous heading changes. In addition, activations relative to the processing of future path cues (Field et al., 2007; Billington et al., 2010; 2013) have been found in the SPL extending medially into the precuneus, in the medial intraparietal sulcus (mIPS) and in the cingulate sulcus, where hPEc, IPSmot and CSv are respectively located. Present results about a preference for forward direction of motion compared to backward direction found in some regions confirm the importance of exploring differences in sensitivity between forward and backward motion in studying the neural basis of visually-guided locomotion control. These results are in line with an enhanced parietal activity (likely involving many of the regions investigated in the present work) during forward than backward stepping observed in a very recent EEG study (Berchicci et al., 2020). Also the preference for locomotion-compatible curved path found in most of the regions tested here suggests that these areas are involved in the visual guidance of locomotion. Indeed, controlling locomotion mainly means controlling changes in the direction of self-motion. This claim is also supported by a recent behavioral study showing that the execution of locomotion-related actions like a forward footstep is facilitated by processing peripheral locations of the visual field (which correspond to the spatial positions we move to during heading changes), likely with the adaptive function of fostering spatial exploration of the surrounding environment by means of locomotion (Di Marco et al., 2019).

Egomotion visual area PIC (white-colored region in Figure 4A) does not show a preference for either curved paths or forward motion. This is in line with PIC functional properties. Indeed, even if this region responds to egomotion-compatible optic flow (Sunaert et al., 1999; Orban et al., 2003; Antal et al., 2008; Cardin & Smith, 2010; Frank et al., 2014; 2016; Uesaki & Ashida, 2015; Serra et al., 2019; Pitzalis et al., 2020), it also responds to vestibular inputs (for a review see Frank & Greenlee, 2018), hence it is supposed to encode any kind of body shift. For example, it has been shown that this region is sensitive to both linear and angular vestibular stimuli (Fasold et al., 2002; Smith et al., 2012; Frank et al., 2014; 2016; Billington & Smith, 2015). Thus, it is predictable that this region does not show a preference for linear or curved and forward or backward visual feedback of such body shifts.

Interestingly, two recent studies of our lab (Pitzalis et al., 2019; Serra et al., 2019) have observed that somatomotor regions hPEc, hPE, S-I and egomotion visual areas CSv, pCi, PIC (but not V6+, V3A, IPSmot) respond to long-range leg movements and are functionally connected with the medial portion of the sensorimotor cortex, where lower limbs are represented. Some of these regions responding to leg movements are part of the dorsomedial visual stream, which is implicated in monitoring actions in space (Galletti & Fattori, 2018; Huang & Sereno, 2018). Thus, putting together present and previous findings, we hypothesize that hPEc, hPE, S-I, CSv and pCi (responding to leg movements) are involved in guiding heading changes in the environment (in both forward and backward motion) during leg-related actions, also including locomotion. To this aim, it is possible that these areas integrate visual motion and leg-related somatomotor signals

and feed such multisensory information into the motor system. Moreover, CSv and pCi may also contribute to visually-guided locomotion control (during forward motion) with a fine visual analysis of the external world. On the other hand, we hypothesized that V6+, V3A and IPSmot, the areas not responding to leg movements, participate in the analysis of visual aspects of egomotion (path curvature and/or motion direction) with no direct involvement in controlling leg-related actions such as locomotion. All these regions have been for example proposed to be involved in flow parsing, that is the capability to subtract self-motion components from retinal motion signals with the aim to extract object motion information (Galletti & Fattori, 2003; Pitzalis et al., 2015; 2020; Field et al., 2020). It is also possible that V6+ and IPSmot, part of the dorso-medial visual stream, play a role in the visual guidance of locomotion by providing the motor regions with visual information (about forward motion/visual environment and/or heading changes/direction of self-motion) which are useful for action planning, as suggested by Galletti and colleagues (Galletti et al., 2003, Galletti & Fattori, 2018). In contrast, V3A belongs to the dorsolateral visual stream which is thought to be responsible for a stable representation of the external environment (Galletti & Fattori, 2018). Thus, it is possible that this region is particularly engaged in maintaining perceptual stability of the external visual world during a visual stimulation compatible with forward locomotion. Interestingly, Sherrill et al. (2015) observed that V6+ and V3A are more functionally connected with PPA and RSC during first-person navigation, suggesting that they may extract visual motion information from optic flow to be sent to place-selective regions in order to update spatial position during navigation. In addition, we recently found that V3A is specialized in encoding not only egomotion-relevant, but also scene-relevant information, likely for the control of navigation in a structured environment (Sulpizio et al., 2020b). Overall, it is worth to note that different response profiles observed across V6+, V3A and IPSmot confirm the hypothesis that each motion-sensitive area is particularly involved in the analysis of different aspects of visual motion (Galletti & Fattori, 2018). Such a wide cortical network of egomotion-sensitive regions, well different in their anatomical location and functional profiles, might underlie multisensory integration processes of sensory information from different modalities for self-motion processing. This may be supported by a white matter tract called SIPS (Stratum proprium of InterParietal Sulcus; Uesaki et al., 2018), connecting the superior and inferior parts of the parietal cortex, whose endpoints correspond to areas PIC in the ventro-medial surface, VIP in the dorso-lateral surface and the cortical territory hosting hPEc, hPE and pCi in the medial surface.

4.1 Multivariate approach: Representational similarity analysis

Beside the ROIs preferences for a specific direction and/or path curvature, we also verified whether forward and backward directions and different path curvatures are underlain by different neural patterns. From the univariate analysis we observed, as described above, that some regions showed a preference for forward and/or curved motion. From the multivariate analysis we found that in all the tested regions, even if with different statistical significance, distance in neural representational space between activity patterns associated with different path curvatures resembles distance between path curvatures in physical space, in a greater extent for forward than for backward direction. We also observed that neural activation patterns associated with path curvatures in forward direction were more similar than those associated with path curvatures in backward direction. These results indicate that all ROIs, even if at different extent, are sensitive to different path curvatures (i.e., for example, curved path to the left and curved path to the right), especially in case of forward direction. Moreover, results demonstrate that different neural representations underlie forward and backward motion. This confirms that forward and backward

directions of motion are separately encoded and are qualitative distinct cues to self-motion likely conveying different kinds of information as hypothesized above.

4.2 Visual responses in leg-related somatomotor regions: hPEc, hPE and S-I

Macaque PEc is primarily a somatomotor region but it also contains visual neurons sensitive to optic flow and selective for positions of the focus of expansion, indicating that this region could participate in self-motion encoding (Battaglia-Mayer et al., 2001; Raffi et al., 2002; 2010; 2011; 2014). In agreement with monkey data, human PEc shows a significant response to egomotion-compatible visual stimuli (Pitzalis et al., 2019). Macaque PE and S-I are somatosensory regions which host somatotopic representations of the entire body and do not contain a relevant number of visual neurons (e.g., Nelson et al, 1980; Sakata et al., 1973; Mountcastle et al., 1975; De Vitis et al., 2019). Human PE, however, shows a marginally significant response to egomotion-compatible visual stimuli (Pitzalis et al., 2019) and may correspond to the leg representation of the somatosensory parietal homunculus which, notably, overlaps retinotopic visual maps (Huang et al., 2012). Human S-I did not significantly respond to egomotion-compatible stimuli (Pitzalis et al., 2019), nor it overlapped retinotopic visual maps (Huang et al., 2012). In the present study we found that all three leg-related somatomotor regions hPEc, hPE and S-I show a visual preference for a curved path compared to a linear path. This result is compatible with macaque and human evidence about the presence of visual responses in PEc and, partly, in PE, but it is in striking contrast with the well-known functional properties of S-I neurons, that are exclusively modulated by somatosensory inputs. One possibility is that the visual information of curved path flow field provides a visual feedback typically associated with active stimulation of leg joints during self-motion. It could be that the strong visual stimulation alone is able to evoke a response in somatosensory neurons of S-I (and maybe also in those of hPE) even in the absence of actual limb involvement, thanks to connections with visual egomotion regions (Serra et al., 2019). Indeed, while moving on a curved path there is a wider involvement of joints, muscles and postural adjustments compared to linear path. In particular, in such a situation hips are continuously stimulated during body rotation. Notably, the S-I region defined here is the leg-related dorsomedial portion of S-I (BA3b), excluding more lateral parts of S-I that represent other body parts. Interestingly, in line with recent evidence about response to stimuli from other modalities in primary sensory cortices (e.g., Driver & Noesselt, 2008; Bieler et al., 2017), some fMRI studies revealed that S-I sensitivity can also be modulated by visual input, since perceiving touch and observing touch elicited topographically overlapping activity (e.g., Kuehn et al., 2014; 2018). Here, it could be that we are observing a similar resonance effect, where S-I activity is triggered solely by the visual stimulus typically functionally paired to the somatomotor stimulation of the lower limbs.

4.3 General considerations

One may argue that differential preference in our ROIs for curved paths vs linear paths and for forward direction vs backward direction may also be imputed to differences in local motion rather than in global motion. However, even if this cannot be ruled out, some considerations make this argument unlikely. First, it should be considered that the experimental design included also an additional condition, i.e. random motion, which is the typical example of local motion as opposed to global motion. This condition has been used as a high-level baseline and subtracted out from all the experimental conditions in order to let ROIs sensitivity to global motion strongly emerge. Hence, differential activity in ROIs should be mainly interpreted net of contribution of local

20

motion. Finally, it is worth noting that no differences have been observed in the opposite direction (i.e., a preference for linear paths or for backward direction) which may have also been expected whether the effects described in the present study were ascribed to local motion.

Present findings might expand the current application of virtual reality tool for gait rehabilitation. Since we found here that the passive visual perception of our visual stimuli is able to activate several leg-related cortical regions (including even the primary somatosensory cortex), a novel therapeutic strategy may approach gait impairment from a perceptual point of view by employing locomotion-compatible optic flow stimuli, especially in forward direction and curved paths, by means of immersive virtual reality (that can stimulate also the very far periphery of the visual field). This could be relevant for example in Parkinson's disease (PD) (Canning et al., 2020), which also manifests deficits in optic flow perception that can affect locomotion control (Halperin et al., 2020). Indeed, it has been found that in PD patients during passive viewing of forward motion, activations of egomotion-related cortical network, also including V6, V3A and CSv, are reduced (Putcha et al., 2014; van der Hoorn et al., 2014) and that perception of visual motion cues facilitates locomotion (Azulay et al., 1999). Our findings about a differentiated role of egomotion- and leg-related in the visual guidance of locomotion might be relevant also for the assessment of rehabilitation protocols, identifying the neurobiological correlates of the therapeutic actions (i.e., significant clinical improvements). This makes recommendations for future research using a virtual-reality fMRI task on locomotion in such clinical populations with the aim of testing how gait/balance rehabilitation is able to evoke brain function changes.

5. Conclusions

The present study reveals differential functional profiles among both somatomotor regions and egomotion areas with relation to locomotion-relevant visual parameters, such as path curvature and self-motion direction. Specifically, these regions show a preference for curved paths and/or forward direction of motion, indicating that they could be differently involved in the visual guidance of locomotion. Some of the tested areas (somatomotor regions hPEc, hPE, S-I and egomotion areas CSv and pCi) also respond to leg movements and are functionally connected with the sensorimotor cortex representing lower limbs (Pitzalis et al., 2019; Serra et al., 2019). We hypothesize that they are involved in controlling changing direction of self-motion during locomotion by integrating visual and proprioceptive signals from lower limbs and by projecting integrated signals to the motor system.

Funding

Declaration of Competing Interest

The authors declare that they have no known competing financial interests or personal relationships that could have appeared to influence the work reported in this paper.

References

Antal, A., Baudewig, J., Paulus, W., & Dechent, P. (2008). The posterior cingulate cortex and planum temporale/parietal operculum are activated by coherent visual motion. *Visual Neuroscience*, 25(1), 17–26. http://doi.org/10.1017/S0952523808080024

Azulay, JP., Mesure, S., Amblard, B., Blin, O., Sangla, I., & Pouget, J. (1999). Visual control of locomotion in Parkinson's disease. *Brain,* 122, 111–120. https://doi.org/10.1093/brain/122.1.111

Bakola, S., Gamberini, M., Passarelli, L., Fattori, P., & Galletti, C. (2010). Cortical connections of parietal field PEc in the macaque: Linking vision and sensation for the control of limb action. *Cereb Cortex,* 20, 2592–2604

Battaglia-Mayer, A., Ferraina, S., Genovesio, A., Marconi, B., Squatrito, S., Molinari, M., Lacquaniti, F., & Caminiti, R. (2001). Eye-hand coordination during reaching. II. An analysis of the relationships between visuomanual signals in parietal cortex and parieto-frontal association projections. *Cereb Cortex*, 11, 528–544. https://doi.org/10.1093/cercor/11.6.513

Beintema, J. A. & van den Berg, A. V. (1996). Heading detection using motion templates and eye velocity gain fields. *Vision Res.*, 38, 2155–2179

Berchicci, M., Russo, Y., Bianco, V., Quinzi, F., Rum, L., Macaluso, A., Committeri, G., Vannozzi, G., Di Russo, F. (2020). Stepping forward, stepping backward: a movement-related cortical potential study unveils distinctive brain activities. *Behavioral Brain Research*, 388, 112663. http://doi.org/10.1016/j.bbr.2020.112663

Bertin, R. J., Isra̍el, I., & Lappe, M. (2000). Perception of two-dimensional, simulated ego-motion trajectories from optic flow. *Vision Res.*, 40(21), 2951–2971

Bieler, M., Sieben, K., Cichon, N., Schildt, S., Ro̍der, B., & Hanganu-Opatz, IL. (2017). Rate and temporal coding convey multisensory information in primary sensory cortices. *eNeuro*, 4, ENEURO.0037–17.2017

Billington, J., Field, D.T., Wilkie, R.M., & Wann, J.P. (2010). An fMRI study of parietal cortex involvement in the visual guidance of locomotion. *J Exp Psychol Hum Percept Perform*, 36, 1495–1507

Billington, J., Wilkie, R.M. & Wann, J.P. (2013). Obstacle avoidance and smooth trajectory control: neural areas highlighted during improved locomotor performance. *Front. Behav. Neurosci.*, 7: 9 https://doi.org/10.3389/fnbeh.2013.00009

Billington, J., & Smith, A. T. (2015). Neural Mechanisms for Discounting Head-Roll-Induced Retinal Motion. *Journal of Neuroscience*, *35*(12), 4851–4856. http://doi.org/10.1523/JNEUROSCI.3640-14.2015

Brainard, D. H. (1997). The Psychophysics Toolbox. *Spatial Vision,* 10, 433-436. http://psychtoolbox.org/credits/
[http://color.psych.upenn.edu/brainard/papers/Psychtoolbox.pdf]

Bremmer, F., Schlack, A., Shah, N. J., Zafiris, O., Kubischik, M., Hoffmann, K.P..Fink, G. R. (2001). Polymodal Motion Processing in Posterior Parietal and Premotor Cortex. *Neuron*, 29, 287–296. http://doi.org/10.1016/S0896-6273(01)00198-2

Bremmer, F., Duhamel, J. R., Ben Hamed, S., & Graf, W. (2002). Heading encoding in the macaque ventral intraparietal area (VIP). *European Journal of Neuroscience*, 16(8), 1554–1568. http://doi.org/10.1046/j.1460-9568.2002.02207.x

Bremmer, F. (2011). Multisensory space: from eye-movements to self-motion. *The Journal of Physiology*, 589(4), 815–823. http://doi.org/10.1113/jphysiol.2010.195537

Breveglieri, R., Galletti, C., Gamberini, M., Passarelli, L., & Patrizia, F. (2006). Somatosensory Cells in Area PEc of Macaque Posterior Parietal Cortex. *J Neurosci*, 26, 3679–3684

Breveglieri, R., Galletti, C., Monaco, S., & Fattori, P. (2008). Visual, somatosensory, and bimodal activities in the macaque parietal area PEc. *Cereb Cortex*, 18, 806–16

Britten, K. H. (2008). Mechanisms of self-motion perception. *Annu. Rev. Neurosci.*, 31, 389– 410

Canning, C.G., Allen, N.E., Nackaerts, E., Paul, S.S., Nieuwboer, A., & Gilat, M. (2020). Virtual reality in research and rehabilitation of gait and balance in Parkinson disease. *Nat Rev Neurol*, 16, 409– 425. https://doi.org/10.1038/s41582-020-0370-2

Cardin, V., & Smith, A. T. (2010). Sensitivity of human visual and vestibular cortical regions to egomotion-compatible visual stimulation. *Cerebral Cortex*, 20(8), 1964–1973. http://doi.org/10.1093/cercor/bhp268

Chen, A., DeAngelis, G. C., & Angelaki, D. E. (2011a). Convergence of vestibular and visual self-motion signals in an area of the posterior sylvian fissure. The Journal of Neuroscience : *The Official Journal of the Society for Neuroscience*, 31(32), 11617–11627. http://doi.org/10.1523/JNEUROSCI.1266-11.2011

Chen, A., DeAngelis, G. C., & Angelaki, D. E. (2011b). Representation of Vestibular and Visual Cues to Self-Motion in Ventral Intraparietal Cortex. Journal of Neuroscience, 31(33), 12036–12052. http://doi.org/10.1523/JNEUROSCI.0395-11.2011

Cottereau, B., Smith, A.T., Rima, S., Fize, D., Héjja-Brichard, Y., Renaud, L., Lejards, C., Vayssière, N., Trotter, Y., Durand, JP. (2017). Processing of Egomotion-Consistent Optic Flow in the Rhesus Macaque Cortex, *Cerebral Cortex*, 27, Issue 1, 330–343. https://doi.org/10.1093/cercor/bhw412

Cutting, J. E., Vishton, P. M., Fluckiger, M., Baumberger, B., & Gerndt, J. D. (1997). Heading and path information from retinal flow in naturalistic environments. *Perception & Psychophysics*, 59, 426–441.

Dale, A.M., Fischl, B., Sereno, M.I. (1999). Cortical surface-based analysis: I. Segmentation and surface reconstruction. *NeuroImage,* 9, 179–194.

Desikan, RS., Ségonne, F., Fischl, B., Quinn, BT., Dickerson, BC., Blacker, D., Buckner, RL., Dale, A.M., Maguire, RP., Hyman, BT. (2006). An automated labeling system for subdividing the human cerebral cortex on MRI scans into gyral based regions of interest. *Neuroimage*, 31, 968-980.

De Vitis, M., Breveglieri, R., Hadjidimitrakis, K., Vanduffel, W., Galletti, C., & Fattori, P. (2019). The neglected medial part of macaque area PE: segregated processing of reach depth and direction. *Brain Struct Funct,* 224, 2537– 2557. https://doi.org/10.1007/s00429-019-01923-8

Di Marco, S., Tosoni, A., Altomare, E.C., Ferretti, G., Perrucci, M.G., & Committeri, G. (2019). Walking-related locomotion is facilitated by the perception of distant targets in the extrapersonal space. *Sci Rep*, 9, 9884. https://doi.org/10.1038/s41598-019-46384-5

Driver. J, & Noesselt. T. (2008). Multisensory interplay reveals crossmodal influences on 'sensory-specific' brain regions, neural responses, and judgments. *Neuron.*, 57(1), 11-23. https://doi.org/10.1016/j.neuron.2007.12.013.

Duffy, CJ., & Wurtz, RH. (1991). Sensitivity of MST neurons to optic flow stimuli I A continuum of response selectivity to large-field stimuli. *J Neurophysiol*, 65(6), 1329-45. https://doi.org/10.1152/jn.1991.65.6.1329

Duffy, CJ., & Wurtz, RH. (1995). Response of monkey MST neurons to optic flow stimuli with shifted centers of motion. *J Neurosci.*, 15(7), 5192-208.

von Economo, C. & Koskinas, G. The Cytoarchitectonics of the Adult Human Cortex (Springer, 1925)

Fan, RH., Liu, S., DeAngelis, GC., & Angelaki, DE. (2015). Heading tuning in Macaque Area V6. *J Neurosci.*, 35, 16303–16314.

Fasold, O., von Brevern, M., Kuhberg, M., Ploner, C. J., Villringer, A., Lempert, T., & Wenzel, R. (2002). Human Vestibular Cortex as Identified with Caloric Stimulation in Functional Magnetic Resonance Imaging. *NeuroImage*, 17(3), 1384–1393. http://doi.org/10.1006/nimg.2002.1241

Field, D. T., Wilkie, R. M., and Wann, J. P. (2007). Neural systems in the visual control of steering. J. *Neurosci.*, 27(30):8002–8010

Field, D. T., Inman, L. A., & Li, L. (2015). Visual processing of optic flow and motor control in the human posterior cingulate sulcus. *Cortex*, 71, 377–389. http://doi.org/10.1016/j.cortex.2015.07.014

Field, D. T., Biagi, N., & Inman, L. A. (2020). The role of the ventral intraparietal area (VIP/pVIP) in the perception of object-motion and self-motion. *NeuroImage*, 213:116679. http://doi.org/10.1016/j.neuroimage.2020.116679

Fischer, E., Bülthoff, H. H., Logothetis, N. K., & Bartels, A. (2012). Visual motion responses in the posterior cingulate sulcus: A comparison to V5/MT and MST. *Cerebral Cortex*, 22(4), 865–876. https://doi.org/10.1093/cercor/bhr154

Fischl, B., Sereno, M. I., & Dale, A. M. (1999a). Cortical surface-based analysis: II. Inflation, flattening, and a surface-based coordinate system. *NeuroImage*, 9(2), 195–207. http://doi.org/10.1006/nimg.1998.0396

Fischl, B., Sereno, M.I., Tootell, R.B.H., & Dale, A.M. (1999b). High-resolution intersubject averaging and a coordinate system for the cortical surface. *Human brain mapping,* 8, 272-284. https://doi.org/10.1002/(SICI)1097-0193(1999)8:4<272::AID-HBM10>3.0.CO;2-4

Frank, S.M., Baumann, O., Mattingley, J.B., & Greenlee, M.W. (2014). Vestibular and visual responses in human posterior insular cortex. *Journal of Neurophysiology*, 112, 2481–91.

Frank, S.M., Wirth, A.M., & Greenlee, M.W. (2016). Visual-vestibular processing in the human sylvian fissure. *Journal of Neurophysiology*, 116(2), 263–271. http://doi.org/10.1152/jn.00009.2016

Frank, S.M., & Greenlee, M.W. (2018). The parieto-insular vestibular cortex in humans: More than a single area? *Journal of Neurophysiology*, 120(3), 1438–1450.

Furlan, M., Wann, J.P., & Smith, A.T. (2014). A representation of changing heading direction in human cortical areas pVIP and CSv. *Cerebral Cortex*, 24(11), 2848–2858. http://doi.org/10.1093/cercor/bht132

Galletti, C., Fattori, P., Battaglini, PP., Shipp, S., & Zeki, S. (1996.) Functional demarcation of a border between areas V6 and V6A in the superior parietal gyrus of the macaque monkey. *Eur J Neurosci*, 8, 30–52.

Galletti, C., & Fattori, P. (2003). Neuronal mechanisms for detection of motion in the field of view. *Neuropsychologia*, 41(13), 1717–1727. http://doi.org/10.1016/S0028-3932(03)00174-X

Galletti, C., Kutz, D. F., Gamberini, M., Breveglieri, R., & Fattori, P. (2003). Role of the medial parieto-occipital cortex in the control of reaching and grasping movements. *Exp. Brain Res.*, 153, 158–170.

Galletti, C., & Fattori, P. (2018). The dorsal visual stream revisited: Stable circuits or dynamic pathways? *Cortex*, 98, 1–15. http://doi.org/10.1016/j.cortex.2017.01.009

Gamberini, M., Galletti, C., Bosco, A., Breveglieri, R., Fattori, P. (2011). Is the medial posterior parietal area V6A a single functional area? *J Neurosci*, 31(13), 5145–5157. https://doi.org/10.1523/JNEUROSCI.5489-10.2011

Gamberini, M., Dal Bò, G., Breveglieri, R., Briganti, S., Passarelli, L., Fattori, P., & Galletti, C. (2018). Sensory properties of the caudal aspect of the macaque's superior parietal lobule. *Brain Struct. Funct.,* 223, 1863-1879.

Gibson, J. J. (1950). The perception of the visual world. Boston: Houghton Mifflin

Gitelman, D.R., Nobre, aC., Parrish, T.B., LaBar, K.S., Kim, Y.H., Meyer, J.R., & Mesulam, M. M. (1999). A large-scale distributed network for covert spatial attention. *Brain*, 122(6), 1093–1106. https://doi.org/10.1093/brain/122.6.1093

Glasser, M.F., Sotiropoulos, S.N., Wilson, J.A., Coalson, T.S., Fischl, B., Andersson, J.L., Xu, J., Jbabdi, S., Webster, M., Polimeni, J.R., Van Essen, D.C., & Jenkinson, M. (2013). The minimal preprocessing pipelines for the Human Connectome Project. *NeuroImage,* 80, 105–124.

Graziano, M. S. A., & Cooke, D. F. (2006). Parieto-frontal interactions, personal space, and defensive behavior. *Neuropsychologia*, 44(13), 2621–2635. http://doi.org/10.1016/j.neuropsychologia.2005.09.011

Greenlee, M.W., Frank, S.M., Kaliuzhna, M., Blanke, O., Bremmer, F., Churan, J., Cuturi, L.F., MacNeilage, P.R., & Smith, A.T. (2016). Multisensory Integration in Self Motion Perception. *Multisensory Research*, 29(6-7), 525-556. https://doi.org/10.1163/22134808-00002527

Halperin, O., Israeli-Korn, S., Yakubovich, S., Hassin-Baer, S., & Zaidel, A. (2020). Self-motion perception in Parkinson's disease. *Eur J Neurosci*. https://doi.org/10.1111/ejn.14716

Huang, R.S., Chen, C., Tran, A.T., Holstein, K.L., & Sereno, M.I. (2012). Mapping multisensory parietal face and body areas in humans. *Proc Natl Acad Sci USA*, 109, 18114–18119. https://doi.org/10.1073/pnas.1207946109

Huang, R.S., Chen, C.F., & Sereno, M.I. (2015). Neural substrates underlying the passive observation and active control of translational egomotion. *J Neurosci.*, 35(10), 4258-67. DOI: 10.1523/JNEUROSCI.2647-14.2015

Huang, R.S., Chen, C., & Sereno, M.I. (2017). Mapping the complex topological organization of the human parietal face area. *NeuroImage*, 163, 459–470. http://doi.org/10.1016/j.neuroimage.2017.09.004

Huang, R., & Sereno, M.I. (2018). Multisensory and sensorimotor maps, 1st ed, The Parietal Lobe. Elsevier B.V.

Kaas, J.H., Gharbawie, O.A., & Stepniewska, I. (2011). The organization and evolution of dorsal stream multisensory motor pathways in primates. *Front Neuroanat.*, 5, 34. doi: 10.3389/fnana.2011.00034. eCollection

Kim, Y.H., Gitelman, D.R., Nobre, A.C., Parrish, T.B., LaBar, K.S., & Mesulam, M.M. (1999). The Large-Scale Neural Network for Spatial Attention Displays Multifunctional Overlap But Differential Asymmetry. *NeuroImage*, *9*(3), 269–277. http://doi.org/10.1006/nimg.1999.0408

Kriegeskorte, N., Mur, M., & Bandettini, P. (2008). Representational similarity analysis - connecting the branches of systems neuroscience. *Front Syst Neurosci.*, 2, 4. doi: 10.3389/neuro.06.004.2008. eCollection 2008.

Kuehn, E., Mueller, K., Turner, R., & Schu¨tz-Bosbach, S. (2014). The functional architecture of S1 during touch observation described with 7 T fMRI. *Brain Struct Funct,* 219, 119 –140.

Kuehn, E., Haggard, P., Villringer, A., Pleger, B., & Sereno, M.I. (2018). Visually-Driven Maps in Area 3b. *J Neurosci.,* 38(5), 1295-1310. doi: 10.1523/JNEUROSCI.0491-17.2017.

Kwong, K.K., Belliveau, J.W., Chesler, D.A., Goldberg, I.E., Weisskoff, R.M., Poncelet, B.P., Kennedy, D.N., Hoppel, B.E., Cohen, M.S., Turner, R. (1992). Dynamic magnetic resonance imaging of human brain activity during primary sensory stimulation. *Proc Natl Acad Sci USA*, 89, 5675–5679

Lappe, M., & Rauschecker, J.P. (1993). A neural network for the processing of optic flow from ego-motion in man and higher mammals. *Neural Comp.,* 5(3), 374–391.

Lappe, M., Bremmer, F., Pekel, M., Thiele, A., & Hoffmann, K. P. (1996). Optic flow processing in monkey STS: a theoretical and experimental approach. *J. Neurosci.,* 16(19), 6265–6285.

Lappe, M., Bremmer, F., & van den Berg, A. V. (1999). Perception of self-motion from visual flow. *Trends Cogn. Sci.,* 3(9), 329–336.

Li, L., Chen, J., & Peng, X. (2009). Influence of visual path information on human heading perception during rotation. *J Vis.*, 9(3), 29. doi: 10.1167/9.3.29

Li, L., & Cheng, J.C. (2011a). Perceiving path from optic flow. *J Vis.*, 11(1), 22. doi: 10.1167/11.1.22

Li, L., & Cheng, J.C. (2011b). Heading but not path or the tau-equalization strategy is used in the visual control of steering toward a goal. *J Vis.*, 11(12), 20. doi: 10.1167/11.12.20

Li, L., Stone, L.S., & Chen, J. (2011). Influence of optic-flow information beyond the velocity field on the active control of heading. *J. Vis.,* 11(4), 1–16.

Li, L. & Warren, W.H.J. (2002). Retinal flow is sufficient for steering during observer rotation. *Psychol. Sci.,* 13(5), 485–491.

Mangan, A.P., & Whitaker, R.T. (1999). Partitioning 3D surface meshes using watershed segmentation. *IEEE Transactions on Visualization and Computer Graphics*, 5(4), 308–321.

Marigold, D.S. (2008). Role of peripheral visual cues in online visual guidance of locomotion. *Exercise and Sport Sciences Reviews*, 36(3), 145–51. http://doi.org/10.1097/JES.0b013e31817bff72

Marigold, D.S., Patla, A.E. (2008). Visual information from the lower visual field is important for walking across multi-surface terrain. *Exp Brain Res*, 188, 23–31. https://doi.org/10.1007/s00221-008-1335-7

Mesulam, M.M. (1999). Spatial attention and neglect: parietal, frontal and cingulate contributions to the mental representation and attentional targeting of salient extrapersonal events. *Philosophical Transactions of the Royal Society B: Biological Scienc*es, 354(1387), 1325–1346. http://doi.org/10.1098/rstb.1999.0482

Mountcastle, V.B., Lynch, J.C., Georgopoulos, A., Sakata, H., & Acuña, C. (1975). Posterior parietal association cortex of the monkey: command function for operations within extrapersonal space. *J Neurophysiol*, 38, 871–908.

Nelson, R.J., Sur, M., Felleman, D.J., & Kaas, J.H. (1980). Representations of the body surface in postcentral parietal cortex of Macaca fascicularis. *J. Comp. Neurol.*, 192, 611–643. https://doi.org/10.1002/cne.901920402

Oldfield, R.C. (1971). The assessment and analysis of handedness: The Edinburgh inventory. *Neuropsychologia*, 9, 97–113.

Orban, G.A., Fize, D., Peuskens, H., Denys, K., Nelissen, K., Sunaert, S., Todd, J., & Vanduffel, W. (2003). Similarities and differences in motion processing between the human and macaque brain: Evidence from fMRI. *Neuropsychologia*, 41(13), 1757-1768.

Paolini, M., Distler, C., Bremmer, F., Lappe, M., & Hoffmann, K. P. (2000). Responses to continuously changing optic flow in area MST. *J. Neurophysiol.*, 84(2), 730–743.

Pelli D.G. (1997). The VideoToolbox software for visual psychophysics: transforming numbers into movies. *Spat Vis.*, 10(4), 437-42.

Penfield, W., 1950. The Cerebral Cortex of The Man. MacMillan, New York

Perrone, J. A., & Stone, L. S. (1994). A model of self-motion estimation within primate extrastriate visual cortex. *Vision Res.,* 34(21), 2917–2938.

Pitzalis, S., Galletti, C., Huang, R.S., Patria, F., Committeri, G., Galati, G., Fattori, P., & Sereno, M.I. (2006). Wide-field retinotopy defines human cortical visual area V6. *J. Neurosci.,* 26, 7962–7973

Pitzalis, S., Sereno, M.I., Committeri, G., Fattori, P., Galati, G., Patria, F., & Galletti, C. (2010). Human V6: The medial motion area. *Cereb. Cortex*, 20, 411–424.

Pitzalis, S., Sereno, M.I., Committeri, G., Fattori, P., Galati, G., Tosoni, A., & Galletti, C., (2013a). The human homologue of macaque area V6A. *NeuroImage*, 82, 517–530.

Pitzalis, S., Sdoia, S., Bultrini, A., Committeri, G., Di Russo, F., Fattori, P., Galletti, C., & Galati, G. (2013b). Selectivity to translational egomotion in human brain motion areas. *PLoS One*, 8(4), e60241

Pitzalis, S., Fattori, P., & Galletti, C. (2015). The human cortical areas V6 and V6A. *Vis. Neurosci.*, 32, E007

Pitzalis, S., Serra, C., Sulpizio, V., Di Marco, S., Fattori, P., Galati, G., & Galletti, C., (2019). A putative human homologue of the macaque area PEc. *NeuroImage*, 202, 116092. https://doi.org/10.1016/j.neuroimage.2019.116092

Pitzalis, S., Serra, C., Sulpizio, V., Committeri, G., de Pasquale, F., Fattori, P., Galletti, C., Sepe, R., & Galati, G. (2020). Neural bases of self- and object-motion in a naturalistic vision. *Human Brain Mapping*, 41, 1084-1111. https://doi.org/10.1002/hbm.24862

Power, J.D., Barnes, K.A., Snyder, A.Z., Schlaggar, B.L. & Petersen, S.E. (2012). Spurious but systematic correlations in functional connectivity MRI networks arise from subject motion. *NeuroImage*, 59(3), 2142–2154. http://doi.org/10.1016/j.neuroimage.2011.10.018

Putcha, D., Ross, R.S., Rosen, M.L., Norton, D.J., Cronin-Golomb, A., Somers, D.C., & Stern, C.E. (2014). Functional correlates of optic flow motion processing in Parkinson's disease. *Frontiers in Integrative Neuroscience,* 8(57), 1–7. doi:10.3389/fnint.2014.00057.

Raffi, M., Squatrito, S., & Maioli, M.G. (2002). Neuronal responses to optic flow in the monkey parietal area PEc. *Cereb Cortex*, 12, 639–646.

Raffi, M., Carrozzini, C., Maioli, M.G., & Squatrito, S. (2010). Multimodal representation of optic flow in area PEc of macaque monkey. *Neuroscience*, 171, 1241–55.

Raffi, M., Maioli, M.G., & Squatrito, S. (2011). Optic flow direction coding in area PEc of the behaving monkey. *Neuroscience*, 194, 136–149.

Raffi, M., Persiani, M., Piras, A., & Squatrito, S. (2014). Optic flow neurons in area PEc integrate eye and head position signals. *Neurosci Lett,* 568, 23–28.

Regan, D., & Beverly, K.I. (1982). How do we avoid confounding the direction we are looking and the direction we are moving? *Science*, 215, 194–196.

Sakata, H., Takaoka, Y., Kawarasaki, A., & Shibutani, H. (1973). Somatosensory properties of neurons in the superior parietal cortex (area 5) of the rhesus monkey. *Brain Res.*, 64, 85–102. https://doi.org/10.1016/0006-8993(73)90172-8

Saunders, J.A. (2010). View rotation is used to perceive path curvature from optic flow. *Journal of Vision*, 10 (13), 25.

Sereno, M.I., & Huang, R.S. (2006). A human parietal face area contains aligned head-centered visual and tactile maps. *Nature Neuroscience*, 9(10), 1337–43. http://doi.org/10.1038/nn1777

Serra, C., Galletti, C., Di Marco, S., Fattori, P., Galati, G., Sulpizio, V., & Pitzalis, S. (2019). Egomotion-related visual areas respond to active leg movements. *Human Brain Mapping*, 40, 3174–3191. http://doi.org/10.1002/hbm.24589

Sherrill, K.R., Chrastil, E.R., Ross, R.S., Erdem, U.M., Hasselmo, M.E., & Stern, C.E. (2015). Functional connections between optic flow areas and navigationally responsive brain regions during goal-directed navigation. *NeuroImage*, 118, 386–396. http://doi.org/10.1016/j.neuroimage.2015.06.009

Smith, A.T., Wall, M.B., & Thilo, K.V. (2012). Vestibular inputs to human motion-sensitive visual cortex. *Cerebral Cortex*, 22, 1068–77.

Smith, A.T., Greenlee, M.W., DeAngelis, G.C., & Angelaki, D.E. (2017). Distributed visual–vestibular processing in the cerebral. *Multisensory Research*, 30, 91–120.

Smith, A.T., Beer, A.L., Furlan, M., & Mars, R.B. (2018). Connectivity of the Cingulate Sulcus Visual Area (CSv) in the Human Cerebral Cortex. *Cerebral Cortex*, 28(2), 713-72. http://doi.org/10.1093/cercor/bhx002

Squatrito, S., Raffi, M., Maioli, M.G., & Battaglia-Mayer, A. (2001). Visual motion responses of neurons in the caudal area PE of macaque monkeys*. J. Neurosci.*, 21, RC130*.*

Stone, L.S., & Perrone, J.A. (1997). Human heading estimation during visually simulated curvilinear motion. *Vision Res.*, 37(5), 573-90.

Sulpizio, V., Neri, A., Fattori, P., Galletti, C., Pitzalis, S., & Galati, G. (2020a). Real and imagined grasping movements differently activate the human dorsomedial parietal cortex. *Neuroscience*, 434, 22–34.

Sulpizio, V., Galati, G., Fattori, P., Galletti, C., & Pitzalis, S. (2020b). A common neural substrate for processing scenes and egomotion-compatible visual motion. *Brain Structure and Function*, 225, 2091-2110. https://doi.org/10.1007/s00429-020-02112-8

Sunaert, S., Van Hecke, P., Marchal, G., & Orban, G.A. (1999). Motion-responsive regions of the human brain. *Experimental Brain Research*, 127(4), 355-370.

Tanaka, K., & Saito, H. (1989). Analysis of motion of the visual field by direction, expansion/contraction, and rotation cells clustered in the dorsal part of the medial superior temporal area of the macaque monkey. *J Neurophysiol*, 62(3), 626-41. https://doi.org/10.1152/jn.1989.62.3.626

Tootell, R.B., Mendola, J.D., Hadjikhani, N.K., Ledden, P.J., Liu, A.K., Reppas, J.B., & Dale, A.M. (1997). Functional analysis of V3A and related areas in human visual cortex. *The Journal of Neuroscience: The Official Journal of the Society for Neuroscience*, 17(18), 7060–7078. DOI: https://doi.org/10.1523/JNEUROSCI.17-18-07060.1997

Tosoni, A., Pitzalis, S., Committeri, G., Fattori, P., Galletti, C., & Galati, G. (2015). Resting-state connectivity and functional specialization in human medial parieto-occipital cortex. *Brain Structure and Function*, 220(6), 3307–3321. http://doi.org/10.1007/s00429-014-0858-x

Uesaki, M., & Ashida, H. (2015). Optic-flow selective cortical sensory regions associated with self-reported states of vection. *Frontiers in Psychology*, 6, 775. https://doi.org/10.3389/fpsyg.2015.00775

Uesaki, M., Takemura, H., & Ashida, H. (2018). Computational neuroanatomy of human stratum proprium of interparietal sulcus. *Brain Struct Funct*, 223, 489–507. doi:10.1007/s00429-017-1492-1.

Van Essen, D.C., Glasser, M.F., Dierker, D.L., Harwell, J., & Coalson, T. (2012). Parcellations and hemispheric asymmetries of human cerebral cortex analyzed on surface-based atlases. *Cerebral Cortex*, 22, 2241–2262.

- van der Hoorn, A., Renken, R.J., Leenders, K.L., & de Jong, B.M. (2014). Parkinson-related changes of activation in visuomotor brain regions during perceived forward self-motion. *PLoS One*, 9, e95861. https://doi.org/10.1371/journal.pone.0095861

Wada, A., Sakano, Y., & Ando, H. (2016). Differential responses to a visual self-motion signal in human medial cortical regions revealed by wide- view stimulation. *Frontiers in Psychology*, 7, 1–17. https://doi.org/10.3389/fpsyg.2016.00309

Wall, M. B., & Smith, A. T. (2008). The representation of egomotion in the human brain. *Current Biology*, 18(3), 191–194. http://doi.org/10.1016/j.cub.2007.12.053

Warren, W. H. and Hannon, D. J. (1990). Eye movements and optical flow. *J. Opt. Soc. Am. A*, 7(1), 160–169

Warren, W.H.J., Morris, M.W., & Kalish, M. (1988). Perception of translational heading from optical flow. *J. Exp. Psychol. Hum. Percept. Perform*., 14(4), 646–660.

Warren, W.H.Jr. (1998). Visually controlled locomotion: 40 years later. *Ecolog. Psychol*., 10, 177–219.

Warren, W.H., Mestre, D.R., Blackwell, A.W., & Morris, M.W. (1991). Perception of circular heading from optical flow. *J. Exp. Psychol. Hum. Percept. Perform.*, 17(1), 28–43.

CRediT Authors Contribution Statement

Sara Di Marco: Conceptualization, Software, Formal Analysis, Investigation, Writing - Original Draft, Writing - Review & Editing. **Patrizia Fattori:** Conceptualization, Writing - Review & Editing. **Gaspare Galati:** Conceptualization, Software, Writing - Review & Editing. **Claudio Galletti:** Conceptualization, Writing - Review & Editing. **Markus Lappe:** Conceptualization, Writing - Original Draft, Writing - Review & Editing. **Teresa Maltempo:** Formal Analysis, Writing - Review & Editing. **Chiara Serra:** Investigation, Writing - Review & Editing. **Valentina Sulpizio:** Conceptualization, Formal Analysis, Writing - Original Draft, Writing - Review & Editing. **Sabrina Pitzalis:** Conceptualization, Supervision, Project administration, Writing - Original Draft, Writing - Review & Editing